

To Be Submitted to the Astronomical Journal

## SUBSTRUCTURE IN CLUSTERS CONTAINING WIDE-ANGLE TAILED RADIO GALAXIES. I. NEW REDSHIFTS

JASON PINKNEY<sup>1</sup>

Department of Astronomy, University of Michigan, 500 Church St., Ann Arbor, MI 89109  
 jpinkney@astro.lsa.umich.edu

JACK O. BURNS<sup>1</sup>

Office of Research and Department of Physics and Astronomy, University of Missouri, Columbia,  
 MO 65211  
 burnsj@missouri.edu

MICHAEL J. LEDLOW<sup>1</sup>

Department of Physics and Astronomy, University of New Mexico, Albuquerque, NM 87131  
 mledlow@gemini.edu

PERCY L. GÓMEZ<sup>1</sup>

Department of Physics and Astronomy, Rutgers University PO Box 849, Piscataway, NJ 08855  
 percy@physics.rutgers.edu

and

JOHN M. HILL

Steward Observatory, University of Arizona, Tucson, AZ 85721-0065  
 jhill@as.arizona.edu

### ABSTRACT

We present new redshifts and positions for 635 galaxies in nine rich clusters containing Wide-Angle Tailed (WAT) radio galaxies. Combined with existing data, we now have a sample of 18 WAT-containing clusters with more than 10 redshifts. This sample contains a substantial portion of the WAT clusters in the VLA 20 cm survey of Abell clusters, including 75% of WAT clusters in the complete survey ( $z \leq 0.09$ ), and 20% of WAT clusters with  $z > 0.09$ . It is a representative sample which should not contain biases other than selection by radio morphology. We graphically present the new data using histograms and sky maps. A semi-automated procedure is used to

---

<sup>1</sup>Former address: Department of Astronomy, New Mexico State University, Box 30001/Dept. 4500, Las Cruces, NM 88003

search for emission lines in the spectra in order to add and verify galaxy redshifts. We find that the average *apparent* fraction of emission line galaxies is about 9% in both the clusters and the field. We investigate the magnitude completeness of our redshift surveys with CCD data for a test case, Abell 690. This case indicates that our galaxy target lists are deeper than the detection limit of a typical MX exposure, and they are 82% complete down to  $R=19.0$ . The importance of the uniformity of the placement of fibers on targets is posited, and we evaluate this in our datasets. We find some cases of non-uniformities which may influence dynamical analyses. A second paper will use this database to look for correlations between the WAT radio morphology and the cluster's dynamical state.

*Subject headings:* galaxies: clusters: general *galaxies: distances and redshifts* galaxies: jets

## 1. Introduction

Wide-angle tailed radio galaxies (WATs) are a powerful type of FR-I (“edge-darkened”, Fanaroff & Riley 1974) radio galaxy associated with first-ranked ellipticals in clusters. Generally, the tails of a WAT bend in a common direction, giving the source an overall V, or C shape (see O'Donoghue et al. 1990 for a radio survey). The mechanism which bends the WATs is poorly understood. Ram pressure caused by motion through the intracluster medium (ICM) was suspected from the time of discovery (Owen and Rudnick 1976). The sticking point in this hypothesis is that  $\approx 1000 \text{ km s}^{-1}$  relative velocities may be required for bending (Eilek et al. 1984), and the host galaxies, typically gE, D and cD, should have much smaller peculiar velocities with respect to their cluster (Malumuth 1992, Burns 1986).

A subcluster merger hypothesis has emerged linking the bent morphology of WATs to the dynamical state of the host cluster (Pinkney et al. 1993, hereafter Pi93, Gomez et al 1997, Roettiger et al. 1996, Loken et al. 1995). In it, the WAT acts as a stationary weathervane, its tails indicating the local flow of ICM in the stormy environment of a cluster-subcluster merger (Burns 1998). If this hypothesis is true, then WAT's should be beacons of cluster mergers.

This hypothesis is difficult to confirm for a *single* cluster: only *radial* peculiar velocities can be ruled out for the WAT galaxy, and the optical signatures of merger can be subtle during post-merger epochs when the ICM motion is still sufficient to shape the WAT (Loken et al. 1995; Pinkney et al. 1996). A large database can provide statistical leverage to test the subcluster-merger hypothesis. In particular, a distribution of WAT radial peculiar velocities can constrain the true WAT velocities, thereby testing the moving-WAT hypothesis. Moreover, the occurrence rate of significant substructure can be compared to a control sample of radio-quiet clusters. In this paper, we present new velocities and positions of over 600 galaxies in 9 WAT clusters. This will

be combined with published data for 9 additional WAT clusters. These data will be used to probe the connection between WAT bending and cluster evolution in paper II. In this paper, section 2 will contain the sample selection criteria. Section 3 describes the observations and reductions. In section 4, we compare our velocities to published ones and discuss the emission line content. Finally, in section 5 we examine the completeness and spatial uniformity of our redshift surveys.

## 2. WAT Cluster Sample Selection

Our primary selection criterion for clusters was radio morphology. Clusters with high resolution radio data were preferred; if there is a morphological trait among WATs that correlates with their dynamical state, we want it to be apparent in the existing maps. We also required galaxies with  $mv \lesssim 18.0$  (Pinkney et al. 1994, hereafter Pi94), and  $\delta < 72^\circ$  for observation with the Steward Observatory 2.3-m telescope + MX spectrometer.

Our resources for sample selection include the VLA survey of 11 WATs by O'Donoghue et al. (1990, hereafter OOE), and the 20 cm VLA Survey of Abell Clusters (Owen & Ledlow 1997 and references therein). This survey contains 38 radio sources informally classified as “WAT” or “WAT?”, 8 of which comprise 2.3% of the complete cluster sample ( $0.0 \leq z \leq 0.09$ ). The survey uses the VLA C-array (1.4 GHz), with adequate resolution (3-15'') to reveal the WAT morphology out to  $z \sim 0.2$ . The VLA maps in OOE generally have higher resolution and sensitivity. Therefore, we attempted to draw as many clusters from this survey as possible. However, several of the OOE clusters are beyond the redshift and declination limits of the MX spectrometer. We emphasize that we did not select WATs by the apparent angle formed by their tails as it might bias the peculiar velocity measurements. Fortunately, the OOE survey included a wide variety of morphologies, so that WATs with strongly bent and weakly bent tails were present.

We obtained new optical spectra for 7 Abell clusters from OOE: A98, A160, A690, A1446, A1684, A2214, and A2462, and for 1 Abell cluster not in OOE, A2220. Together with the published databases for A115 (Beers, Huchra, & Geller 1983), A400 (Beers et al. 1992), A623 and A2304 (Gómez 1998), A1346 (Slinglend et al. 1998), A1940 (Huchra et al. 1992), A1569 (Gomez et al 1997), and A2634 (Pi93, Scoggio et al. 1995), we have redshift databases for 16 Abell clusters with WATs.

In addition, we observed a *poor cluster* containing the WAT 1313+073 (Patnaik et al 1986). We will also include the published database for the poor cluster containing the WAT 1919+479 (Pi94). Both are good examples of the WAT morphology with excellent radio maps available. We argue that inclusion of these poor clusters is appropriate in this study because the X-ray and radio properties of poor and rich clusters overlap (Price et al. 1991, Burns et al. 1996), and redshift-corrected membership counts of poor clusters overlap those of richness class 0 and 1 Abell clusters (Andersen & Owen 1994).

The radio properties of our combined sample of 18 WATs are shown in Table 1. This sample

contains 6/8 (75%) of WAT clusters in the complete 20 cm VLA survey ( $z \leq 0.09$ ), and 7/30 (23%) of the WAT clusters in the high redshift portion of the VLA survey. The ROSAT X-ray data for five of these clusters were discussed in Gómez et al. (1997). The quantities “Extent”,  $r/A_C$ , and  $\log(P_{1400})$  in Table 1 might all conceivably be correlated with global cluster properties. We will return to these in paper II.

### 3. Multifiber Spectroscopy

The spectral observations of cluster galaxies were made with the MX multifiber spectrometer (Hill & Lesser 1986) on the Steward Observatory 2.3-meter telescope. The MX uses mechanical probes to position 2" diameter fibers in the focal plane with 0.5" precision. The useful field diameter is 45'. Up to 32 fibers are assigned to galaxies, while 29 are placed on the sky.

Our initial detector was a TI 800x800 CCD which became unreliable after our Dec. 31, 1991 run (Table 2). For the remaining runs, we used Loral 1200×800 CCDs. The Loral chips had a superior full well capacity, readout noise, and Q.E. (which exceeded 90% at 4000Å). Our first Loral chip had a problem with excessive ‘cosmic rays’ caused by a radioactive coating on the chip. On the next run, the second Loral chip lacked the radioactive coating. However, it had a problem with large gradients in bias which varied with time. This problem was handled in reduction by replacing standard bias subtraction with subtraction of a surface fit to inter-aperture counts. The old 300 lines/mm diffraction grating was switched with a 400 lines/mm grating (4890Å blaze) for the Dec 1992 run. This changed the dispersion from 3.6 to 2.6 Å pix<sup>-1</sup> and the spectral resolution improved from 8.3 Å to 6.1 Å. After two useful runs with the second chip, a third Loral chip was used which had a stable bias level. Some sample spectra from our surveys are shown in Figure 1. The spectral range was nominally reduced to 3800-6900 Å for cross-correlation.

Our basic CCD reduction, spectral extraction and cross-correlation procedures are much the same as in Pi93 and Pi94. Post-correlation reduction includes a new, objective algorithm for combining the velocities produced by 21 templates. This algorithm uses the  $r$  value of the CCF (cross-correlation function, Tonry & Davis 1979), and the number of templates agreeing on the same velocity (within a 600 km s<sup>-1</sup> range) as criteria for including or excluding velocities in an average. We use three categories for a galaxy’s final velocity measurement, category 1 (hereafter C1), those with an average  $r$  value  $\geq 3.5$  and at least 4 templates in agreement; category 2 (hereafter C2), those with  $3.0 \leq r < 3.5$  and at least 4 templates in agreement; and “invalid”, those which do not fall into the above categories. The C2 category includes velocities which are  $\gtrsim 50\%$  likely to be determined from the correct peak in the CCF. Therefore, C2 galaxies can be classed as cluster members or non-members with some accuracy, but should be omitted from analyses of the velocity distribution. The  $r$  value was also used in combining redundant observations of galaxies: spectra with low  $r$  were excluded from the velocity determination if high  $r$  spectra existed. The final velocities and positions are tabulated in Table 3. The fourth and fifth columns contain the C1 and C2 velocities, respectively. Galaxies with invalid measurements, with

no measurements, and stars, are omitted.

To determine the velocity errors (column 6, Table 3), we fitted a curve to the relation between velocity deviation and the  $r$  value of the CCF (similar to Pi94, Hill & Oegerle 1993). We used 251 repeat spectra of galaxies from 4 clusters taken with the Loral CCD systems for this calibration. The resulting fit is  $\epsilon(r) = 486.7(1.0 + r)^{-1}$ . When three or more good spectra were obtained, the standard deviation was used as the velocity error. If the calculated errors were less than 20 km s $^{-1}$ , the final velocity error was set to 20 km s $^{-1}$ . The last two rules also applied to emission line velocities (see §4.2). An emission line redshift would only be adopted if the cross-correlation results had a larger scatter or  $r \lesssim 4.0$ . If only one spectrum existed, the standard deviation of velocities derived from each emission line was used. All C2 velocities were assigned an error of 200 km s $^{-1}$ , to discourage their use for purposes that require greater velocity precision.

#### 4. The WAT Velocity Database

A collage of histograms is shown for our nine new datasets in Figures 2 and 3. It is clear that the WATs are associated with real systems in redshift space. Also, visual inspection of these figures reveals obvious velocity substructure in clusters such as A98, and A160. In Table 4 we summarize the cluster velocity distributions. Here we use the traditional mean and standard deviation and apply them to the velocities within  $\pm 4000$  km s $^{-1}$  of the WAT. These estimators of velocity centroid and dispersion are notoriously poor in the presence of outliers or substructure (Beers et al. 1990). In Paper II, we will account for substructure in the datasets and apply more robust estimators to the velocity distribution.

##### 4.1. Comparison with literature

As a check on our velocity measurements, we have compared our results to those published for A2462 (also called A3897, Katgert et al. 1998) and A98 (Beers, Geller, & Huchra, 1982; Faber & Dressler 1977; Zabludoff et al. 1990) in Table 5. Redshifts for A98 were first obtained by Faber & Dressler 1977 (FD) and were added to by Beers, Geller, & Huchra, 1982 (BGH). The average difference between our velocities and those of BGH and FD combined is -67 km s $^{-1}$ , with  $\sigma=113$  km s $^{-1}$  ( $N=7$ ). This standard deviation is consistent with random errors in velocity of 80 km s $^{-1}$ . Zabludoff et al. (1990) later took the data added by BGH and re-reduced it with a new template. The difference between our velocities and the velocities in Zabludoff et al. are 40 km s $^{-1}$ , with  $\sigma=157$  ( $N=5$ ). Two velocities were measured by Faber & Dressler 1977 and ourselves, but not BGH, they differed by -193 and -132 km s $^{-1}$ .

We wish to add to our dataset the 21 BGH/FD galaxies which we did not observe. The measured zero-point shift (-67 km s $^{-1}$ ) is only marginally inconsistent with no shift ( $1.6\sigma$ ), so we will not attempt to correct for it. We have precisely re-measured the positions of the BGH

galaxies on our quick-V frame based on their finding chart. We include them in Table 3, and give them ID's that begin with “0”.

Table 5 compares the 12 velocities in Abell 2462 which were measured by both ENACS (ESO Nearby Abell Cluster Survey) and us. The mean difference (after removing the  $325 \text{ km s}^{-1}$  CMB correction used by ENACS) was  $-98.8 \text{ km s}^{-1}$  with a standard deviation of  $111.2 \text{ km s}^{-1}$ . One velocity, ENACS # 12, was adopted since we had no measurement. The ENACS galaxies are labeled in the notes column of Table 3. Our velocities are in reasonable agreement with published values.

#### 4.2. Emission Line Galaxy Survey

We searched our data for emission line galaxies (ELGs). The primary goals were to strengthen the accuracy of the velocity measurements and to increase cluster membership. The codes in column 7 of Table 3 indicate the presence of emission lines in the spectra.

Emission line redshifts were measured in a two-stage process. The first stage identified potential redshift systems using IRAF-based scripts and a Fortran program. Each spectrum was continuum-subtracted and its positive features over  $\approx 2 \times \text{RMS}$  were identified. Each feature was fitted with a Gaussian. The features were then searched for redshift systems containing any 2 or more of 15 lines produced by [OI], [OII], [NeIII], [OIII], [NI], [NII], [SII] or the Balmer series. To reduce spurious results, the program rejected features that were: 1) too close to 4 major night sky lines, 2) too thin ( $\text{FWHM} \leq 3.8 \text{ \AA}$ ), 3) too wide ( $\text{FWHM} \geq 25 \text{ \AA}$ ), or 4) too low in flux ( $< 20 \text{ DN}$ ). The program ranked the systems based upon how well their features agree in redshift, and the number of features they contain.

In the second stage, the output from the automated search was used as a guide to judge the final validity of each system. We judged redshift systems based on the line id's, fluxes, FWHM, redshift agreement with each other and agreement with cross-correlation results. We also visually inspected the candidates to look for lines missed by the automated search, and to choose between the redshift systems. A spectrum had to have at least 2 lines of [OII], [OIII]  $\lambda 5007$ , H $\beta$ , or H $\alpha$  to be acceptable, while lines of [OI], [OIII]  $\lambda 4363$ , [NeIII], and [NI] were insufficient. Moreover, we expected line ratios to be typical of astrophysical environments, e.g., the [OIII]  $\lambda 4959$  line flux should not be much larger than that of  $\lambda 5007$ , and H $\beta$  should not be larger than H $\alpha$ . Convincing lines typically had  $\text{FWHM} \gtrsim 6 \text{ \AA}$  and rarely exceeded  $15 \text{ \AA}$ . The sensitivity limit in equivalent width was roughly -5 to  $-10 \text{\AA}$ . Real line systems typically had internal scatter  $\lesssim 100 \text{ km s}^{-1}$ . An example of a convincing ELG spectrum is shown in Fig 1c.

We show the results of our ELG survey in Table 6. Here we see a range of 0 - 20% in the percentage of cluster members with emission, with an average of 8.6%. As a comparison, Biviano et al. (1997) find  $\approx 16\%$  in the ENACS database, although they have perhaps less stringent criteria (1 emission line is sufficient). Each of our percentages should be considered a lower limit to the

true ELG percentage because many factors reduce our detection of emission lines. The positioning of the H $\alpha$  line within the spectral range was the main factor (see Table 6). Abell 160 has the highest ELG% and this is probably related to the frequent inclusion of H $\alpha$  within the spectral range. Another factor is the confusion of galaxy emission with night sky lines. Some members of A98 and A1446 will have their [OIII] redshifted near  $\lambda 5577$ , and the automated program will reject any line within a window centered on that line. Despite this, the ELG% for A1446 appears high. However, the ELG fraction for non-members in the A1446 field is also high, suggesting that excellent data quality is the cause rather than cluster properties. In general, our data are not sufficiently homogeneous to make direct comparisons between ELG fractions in our clusters. The bottom row of Table 6 indicates that the apparent fraction of ELGs is roughly the same among our member and non-member (“field”) samples. This coincidence results from our particular detection limits for ELG’s and non-ELG’s. Biviano et al. (1997) find an *apparent* fraction of ELGs among the field about  $2\times$  greater than inside clusters (a real field-cluster difference is expected because of morphological segregation). Given that their search criteria are less stringent than ours, their sensitivity to ELG’s is higher in both environments. But the *fraction* of ELGs will be disproportionately higher in the field because it contains mostly spirals. So it is not surprising that our results differ.

## 5. Spatial sampling and magnitude completeness

For many cluster analyses, it is important that the candidate galaxies in the cluster fields are evenly sampled. Radial variations in sampling will result in misrepresentation of the cluster velocity dispersion and mass if there is a non-constant dispersion profile. Azimuthal variations can result in overlooking subclusters that are kinematically distinct. Splotchy sampling in general can cause false positives in substructure tests that are sensitive to bimodality or asymmetry (Pinkney et al. 1996). Thus, one should be aware of the spatial uniformity of one’s cluster redshift survey. Moreover, if one wishes to compare the occurrence rate of substructure in one survey to another, it is desirable to know the depth and area of coverage in both surveys. We will address these issues as follows: first, we describe how our lists of galaxy candidates were created, second, we will estimate the completeness of these lists (hereafter, *MX files*), and third, we will evaluate how evenly we placed fibers on the candidate galaxies.

### 5.1. Candidate galaxy selection

The cluster search fields were roughly square with sides of  $3 h_{75}^{-1}$  Mpc (Table 7 gives dimensions) and centered on the WAT. A digitized image was obtained from the “Quick-V” survey (DSS). Galaxies were selected by inspecting prints of the Palomar Sky Survey (PSS) with a binocular magnifier. Objects were circled on a hardcopy of the DSS image and given priorities to be used in fiber placement. We included galaxies below the magnitude limit for

reliable cross-correlation (estimated from early data). We also included faint, compact objects which showed slight “fuzz” or asymmetry. The poor candidates were given low priorities so that obvious galaxies would be observed first. Coordinates were then measured to  $\lesssim 0.^{\circ}5$  precision on the DSS images using the Guide-star Astrometric Support Package (GASP). These coordinates were assembled into an *MX file* for each cluster. Finally, the MXPACKAGE tasks in IRAF<sup>2</sup> are used to select targets for individual exposures. We iterated on the priorities after observing runs to eliminate the stars.

## 5.2. Completeness of candidate galaxies and depth of spectra

To address the completeness of our *MX files* we used new CCD data obtained for Abell 690 at the M-D-M 1.3-m on Jan 4, 1999. We used a  $2048^2$  STIS CCD with  $0.44.^{\prime\prime}/\text{pix}$ . We obtained 1160 sec of total exposure in each of the V and R filters. The dithered exposures were combined to make a  $14.^{\circ}4 \times 15.^{\circ}0$  image ( $1.15 \times 1.20 h_{75}^{-1} \text{ Mpc}$ ). The gibbous Moon made the images noisy and difficult to flatfield; our limiting magnitude was  $R=21.2$  ( $2.5\sigma$ ). The FWHM of the PSF was about  $1.^{\prime\prime}8$ .

The detection and classification of objects in these frames were done using SExtractor (Bertin & Arnouts 1996) in double-image mode. SExtractor provides a “stelligrity index” (hereafter, *SI*) which corresponds roughly to a confidence limit (1=stellar, 0=non-stellar). SExtractor could rule out stelligrity with 95% confidence ( $SI \leq 0.05$ ) down to  $R=19.0$ . We used an adaptive aperture magnitude which included all but  $\approx 10\%$  of the light for galaxies. A photometric calibration using Landolt standard stars allowed us to set the zeropoint. A comparison to 11 field stars in the USNO\_A01 (Monet et al. 1996) gave a zero point offset of 0.16 mag, which is less than the USNO plate-to-plate errors. We also estimated our scatter to be  $< 0.13$  mag.

The total number of *MX file* objects in the CCD field was 79. SExtractor classified 50 of these as non-stellar, with  $SI \leq 0.2$ , 18 as ambiguous objects ( $0.2 \leq SI \leq 0.8$ ), and 11 as stellar ( $0.8 \leq SI \leq 1.0$ ). The numerous ambiguous and stellar objects mostly appear faint and/or compact on the PSS and were given low priorities. Most of the  $SI \geq 0.8$  objects are stars, but we measured a C1 galaxy velocity for one object with  $SI = 0.98$ . Five more examples of C1 galaxies were found with  $0.2 \leq SI \leq 0.8$ . Had our *MX* candidates been selected based on these *SI* results, several real galaxies would have been omitted. This underscores the possibility that compact galaxies are often overlooked in redshift surveys (Drinkwater et al. 1999). SExtractor also erred in the opposite sense, classifying stars as galaxies, particularly where the PSF distorted near the field edge. The 3 brightest of these were omitted from the following.

The completeness of our A690 *MX file* is plotted in Fig 4. The solid line is the fraction of

---

<sup>2</sup>IRAF is distributed by the National Optical Astronomy Observatories, which is operated by AURA under cooperative agreement with the NSF.

CCD galaxies that are included in the *MX file*. There are 4 omissions in the R=16.75 and 17.25 bins. Two of these galaxies were in fact spotted on the PSS, but failed to be catalogued because of mistakes in bookkeeping. One was excluded from MX because of its proximity to a bright star. One CCD object was overlooked. The fainter, R=17.75 bin is 100% complete. In R=18.75, the completeness of our *MX file* is about 70%, and it quickly drops thereafter. Combining all bins with  $R \leq 19.0$ , the A690 *MX file* is 82% complete. Thus, we find that our method of galaxy selection is also subject to errors, but few of these are oversights.

We suspect that our other *MX files* were not equally deep. Table 7 shows the number of candidate galaxies for each cluster, “ $N_{Cand.}$ ”, which is a measure of how thoroughly the PSS prints were searched for candidates. However, it must be modulated by the the cluster richness count ( $R$ ), search field size (Field), field star density, and redshift (Table 6). It appears that A1684 and A2220 have relatively small candidate lists for their richness, field size, etc., and thus are likely to have lower completeness. In contrast, A2462 has a relatively large  $N_{Cand.}$ .

If all *MX files* are far deeper than the limit of the detector, the variations are inconsequential. We have examined the limit of detection by the 2.3-m + MX using the A690 CCD data. We consider a “detection” to be a spectrum with a reliable (C1) redshift. We do not expect a sharp magnitude limit because the detectability should vary with observing conditions, the compactness and spectral type of the galaxy, etc. We find that, for 1 hour exposures, about 50% of objects with  $18.0 < R < 18.5$  provided C1 redshifts. Below this, the number of C1 results declines rapidly. This suggests a rough limit of  $R \approx 18.5$ . However, our probabilities are boosted in the case of A690 because most of its galaxies were observed repeatedly. Thus,  $R \approx 18.5$  is the limit under the best conditions. For a single exposure in average conditions, the magnitude of 50% probability is probably brighter than  $R \sim 18.0$  (Cf.  $R \approx 17.25$ , Pi94). Since over half of the *MX file* objects in the A690 CCD field were fainter than R=18, our *MX files* appear deeper than the MX limit. Also, our target priorities cause the brightest galaxies to be observed first. Thus, any variations in the depth at which we surveyed the PSS prints should not seriously affect the depth of our detections.

We have shown that the *MX files* are nearly complete down to the detection limit of the instrument ( $R \sim 18.5$ ). But how many objects were actually *observed* to this depth, and how many yielded reliable redshifts? The dotted line in Fig. 4 indicates the fraction of A690 objects with  $SI \leq 0.2$  for which a spectrum was obtained. We have a spectrum for 68% (34/50) of all  $SI \leq 0.2$  objects brighter than R=18.5, and a C1 redshift for 50%. Since this sample defined by SExtractor omits at least 6 galaxies and includes stars, let us take the sample of 79 *MX file* objects contained within the CCD field and remove objects with  $SI \geq 0.2$  and  $R > 18.5$ . Then we have a spectrum for 95% and a C1 redshift for 61%. Lacking a definitive list of galaxies in the field, we estimate that about 60% of the galaxies in A690 have reliable redshifts down to the MX limit (R=18.5).

The other WAT clusters may differ in completeness. Table 7 shows the *sampling percentage* (“%”), or the percentage of *MX file* objects that were observed. For A690, the sampling percentage is 76.4%, which ranks 3rd from highest. The 1st and 2nd ranked percentages are for A1684 and

A2220, but since these have a relatively small number of candidates ( $N_{Cand.}$ ), A690 is probably deeper. A690 had 19 exposures which should boost its completeness considerably. The clusters with the *lowest* sampling percentages, A1446 (42.4%) and A2214 (52.1%), are likely to have lower completeness levels because of the low number of exposures. The cluster with the lowest percentage, A2462 (34.5%), may not be especially incomplete because it has a very large catalog ( $N_{Cand.}=444$ ) for its richness (0).

In summary, the completeness of our A690 *MX file* is 82% down to  $R=19.0$  and other clusters should scale roughly by  $N_{Cand.}$ . The sampling of our well-observed clusters (e.g., A690) is very high (about 95% to  $R=18.5$ ) resulting in reliable redshifts for about 60%. Unfortunately, some of our clusters require more observations for this level of completeness. For example, we are in danger of missing substructures in A1446 and A2214 where the sampling drops below 40% in subregions.

### 5.3. Spatial fairness of sampling

We were concerned with obtaining uniform spatial coverage of our clusters. The priorities we assigned to the objects in our *MX files* were used to control this. MXPACKAGE would reduce the priorities to avoid repetitions in consecutive exposures, and we manually reduced the priorities from night to night to better sample all the galaxies. We further influenced the spatial coverage by the choice of a center star for guiding. This made different regions of the field accessible to the probes. Finally, the density of fiber probes as a function of radius was also adjustable by the user.

We have evaluated how evenly we sampled the candidate galaxies by dividing the cluster search fields into 6 subregions. These subregions are shown in Figure 5 for A690 and A2634. The subregion sampling percentages for each cluster are summarized in Table 7. Abell 1684, and 2214 appear to be undersampled in their centers compared to their outer regions. The difference between these two counts is only significant at the  $1.3$  and  $2.3\sigma$  level, respectively. These are fairly distant clusters with less than 5 exposures, so their cores were not thoroughly probed. Abell 2462 and 2634 are *over-sampled* in the center compared to the outer regions at the  $4.9$  and  $3.1\sigma$  levels, respectively. A2634 also shows a significantly deficient SW quadrant. Abell 160 is marginally over-sampled in the center ( $2.8\sigma$ ). The other clusters (including A690 in Fig. 5) are reasonably evenly sampled. Thus, we find  $3\sigma$  non-uniformities in 2 cases, A2462 and A2634, and 4 other less significant cases: A160, A1684, A2214, and A2220. Even the less severe non-uniformities could influence substructure analysis and velocity dispersion measurements. We will keep this in mind for our analysis in paper II.

## 6. Summary

We have presented new redshifts and positions for galaxies in 9 WAT clusters. Nineteen of our galaxies had published redshifts which are in reasonable agreement with our redshifts (i.e.,

( $\sigma \lesssim 150$ ). A search for emission line galaxies helped contribute cluster redshifts and improve the accuracy of our catalog. Our candidate galaxies for observation were chosen by visual inspection of the PSS. CCD data for Abell 690 indicate that its candidate list (*MX file*) is 82% complete down to R~19.0. Also, 95% of A690 targets are observed, while about 60% of them have reliable redshifts down to the MX detection limit (R~18.5). The fraction of candidates that are *observed* varies from cluster to cluster, and, for 2 clusters, varies strongly between subregions in the cluster. Nevertheless, the dataset is well-suited for measuring WAT peculiar velocities, and can also be used for substructure analyses with attention to the cases with uneven sampling. Paper II will use these data to look for links between the WAT radio morphology and the cluster’s dynamical state.

We would like to thank George Rhee for assistance on the initial observing runs, William Oegerle for providing digitized, “Quick V” survey images which were essential for galaxy astrometry, the Steward Observatory TAC, and Frazer Owen, who kindly made available a listing of sources from the 20 cm VLA Northern Abell Cluster Survey prior to publication. Support was provided for this research by NSF grants AST-9317596, AST-9896039, and NASA grant NAGW-3152 to J. O. B., and by HST grant GO-07388.01 and LTSA grant NAG5-8238 to D. Richstone. Data were obtained (in part) using the 1.3 m McGraw-Hill Telescope of the M-D-M Observatory. This research has made use of the NASA/IPAC Extragalactic Database (NED), which is operated by the Jet Propulsion Laboratory, California Institute of Technology, under contract with the National Aeronautics and Space Administration.

## REFERENCES

- Andersen, V., & Owen, F. N. 1994, AJ, 108, 361
- Beers, T.C., Flynn, K., & Gebhardt, K. 1990, AJ, 100, 32
- Beers, T.C., Gebhardt, K., Huchra, J.P., Forman, W., Jones, C., & Bothun, G. 1992, ApJ, 400, 410
- Beers, T. C., Geller, M. J., & Huchra, J. P. 1982, ApJ, 257, 23
- Beers, T. C., Huchra, J. P., & Geller, M. J. 1983, ApJ, 264, 356
- Bertin, E., & Arnouts, S., 1996, A&AS, 117, 393
- Biviano, A., Katgert, P. Mazure, A., Moles, M., Hartog, R. den, Perea, J.& Focardi, P. 1997, A&A321, 84
- Burns, J. O. 1986, CaJPh, 64, 373
- Burns, J. O., Ledlow, M. J., Loken, C., Klypin, A., Voges, W., Bryan, G. L., Norman, M. L., & White, R. A., 1996, ApJ, 467, L49
- Burns, J. O. 1998, Science, 280, 400
- Drinkwater, M. J., Phillipps, S., Gregg, M. D., Parker, Q. A., Smith, R. M., Davies, J. I., Jones, J. B. & Sadler, E. M. 1999, ApJ, 511, L97
- Eilek, J.A., Burns, J.O., O'Dea, C.P., & Owen, F.N. 1984, ApJ, 278, 37
- Faber, S. M., & Dressler, A. 1977, AJ, 82, 3
- Fanaroff, B.L. & Riley, J.M. 1974, MNRAS, 167, 31
- Gómez, P. L., 1998, Ph.D. Thesis, New Mexico State University
- Gómez, P. L., Pinkney, J., Burns, J. O., Wang, Q., Owen, F. N., & Voges, W. 1997, ApJ, 474, 580
- Hill, J. M. & Oegerle, W. R., 1993, AJ, 106, 831
- Hill, J. M., & Lesser, M.P. 1986, Proc. Soc. Photo-Opt. Instrum. Eng. 627, 693
- Huchra, J. P., Geller, M. J., Clemens, C. M., Tokarz, S. P., and Michel, A., 1992 “The CfA Redshift Catalogue”, Harvard-Smithsonian Center for Astrophysics, Cambridge, MA
- Katgert, P. Mazure, A., den Hartog, R., Adami, C., Biviano, A., & Perea, J. 1998, A&AS, 129, 399
- Loken, C., Roettiger, K., Burns, J.O., & Norman, M. 1995, ApJ, 445, 80L

Malumuth, E. M. 1992, ApJ, 386, 420

Monet, D., Bird, A., Canzian, B., Harris, H., Reid, N., Rhodes, A., Sell, S., Ables, H., Dahn, C., Guetter, H., Henden, A., Leggett, S., Levison, H., Luginbuhl, C., Martini, J., Monet, A., Pier, J., Riepe, B., Stone, R., Vrba, F., Walker, R. 1996, USNO-SA1.0, (U.S. Naval Observatory, Washington DC).

O'Donoghue, A., Owen, F. N., & Eilek, J. A. 1990, ApJS, 72, 75 (OOE)

Owen, F. N., & Rudnick, L. 1976, ApJ, 205, L1

Owen, F. N., White, R. A., & Burns, J. O. 1992, ApJS, 80, 501

Owen, F. N., White, R. A., & Ge, J.P. 1993, ApJS, 87, 135

Owen, F. N., White, R. A., & Thronson, H. A. 1988, AJ, 95, 1

Owen, F. N., & Ledlow, M. J. 1997, ApJS, 108, 41

Owen, F. N., Ledlow, M. J., & Keel, W. C. 1995, AJ, 109, 14

Patnaik, A. R., Malkan, M. A., & Salter, C. J. 1986, MNRAS, 220, 351

Pinkney, J., Burns, J. O., & Hill, J. M. 1994, AJ, 108, 2031 (Pi94)

Pinkney, J., Rhee, G., Burns, J. O., Hill, J. M., Oegerle, W., Batuski, D., & Hintzen, P. 1993, ApJ, 416, 36 (Pi93)

Pinkney, J., Roettiger, K., Burns, J. O., & Bird, C. M. 1996, ApJS, 104, 1

Price, R., Burns, J.O., Duric, N., Newberry, M. V. 1991, AJ, 102, 14

Roettiger, K., Burns, J. O., & Loken, C. 1996, ApJ, 473, 651

Scoggio, M., Solanes, J. M., Giovanelli, R., & Haynes, M. P. 1995, ApJ, 444, 41

Slinglend, k., Batuski, D., Miller, C., Haase, S., & Michaud, K. 1998, ApJS, 115, 1

Tonry, J., & Davis, M. 1979, AJ, 84, 1511

Zabludoff, A. I., Huchra, J. P., & Geller, M. J. 1990, ApJS, 74, 1

### List of Figures

Fig. 1.— Spectra from the MX multifiber spectrometer. The night sky spectrum has been subtracted, but the residuals of prominent lines (marked “ns”) may be visible. a) The WAT in Abell 1684. Note the interference of night sky with Mg b. b) The WAT in Abell 1446. c) A convincing emission line spectrum from A98. d) A galaxy in A98 showing prominent Balmer absorption left of the 4000Å break and slight OII emission indicative of post- or ongoing- star formation.

Fig. 2.— Histograms showing all C1 velocities (see text) measured in the fields of Abell 98, 160, 690, 1446, and 1684. The number of C1 velocities is shown.

Fig. 3.— Histograms showing all C1 velocities measured in the fields of Cl1313+073, Abell 2214, 2220, and 2462. The number of C1 velocities is shown.

Fig. 4.— Plot of completeness vs. SExtractor R magnitude within a 14'4X15' field of Abell 690. Use the left axis for the two completeness curves and the right axis for the triangles and squares. The solid curve is the fraction of SExtractor galaxies ( $SI \leq 0.2$ ) which are in the *MX file* (see text). The dotted curve is the fraction of the SExtractor galaxies which were actually observed by MX. The boxes are the number of SExtractor galaxies in each 0.5-mag bin, while the triangles are the number of those SExtractor galaxies which are also in the *MX file*.

Fig. 5.— Two plots showing the uniformity of spatial sampling for Abell 690 and Abell 2634. The filled circles are candidate galaxies with a spectrum (i.e., “sampled”) and the open circles are candidates without a spectrum. The percentage of candidates observed is labelled inside six sub-regions: four equal-sized quadrants, a region inside of the circle ( $D = 1/2$  field height), and a region outside of the circle. These sampling percentages are given for all of the clusters in Table 7. Note that Abell 2634 is undersampled in the lower right quadrant (Q4) and oversampled in the center.

### List of Tables

Table 1: Radio Properties of WATs.

Table 2: Log of MX Observing Runs.

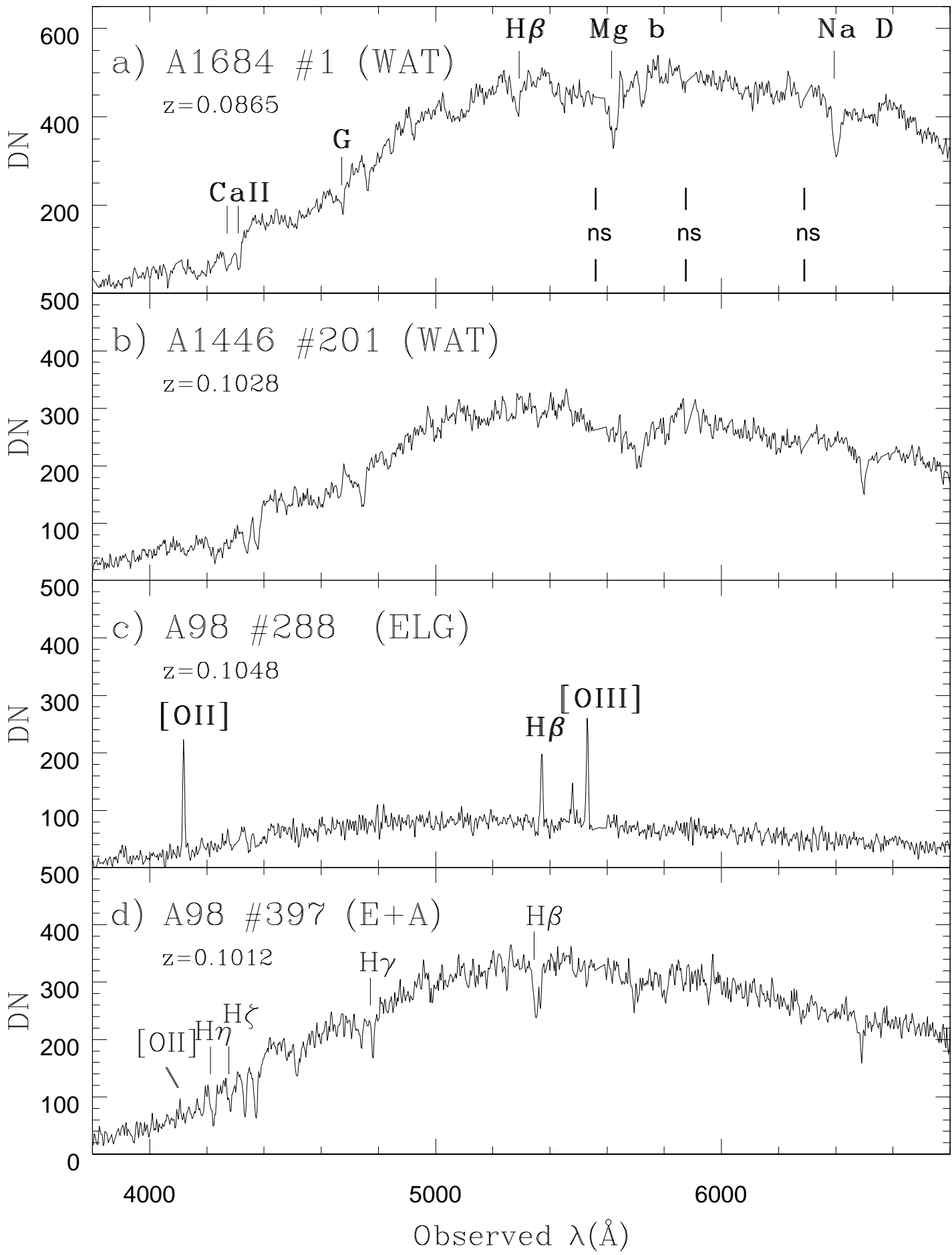
Table 3: Positions and Velocities of WAT cluster galaxies.

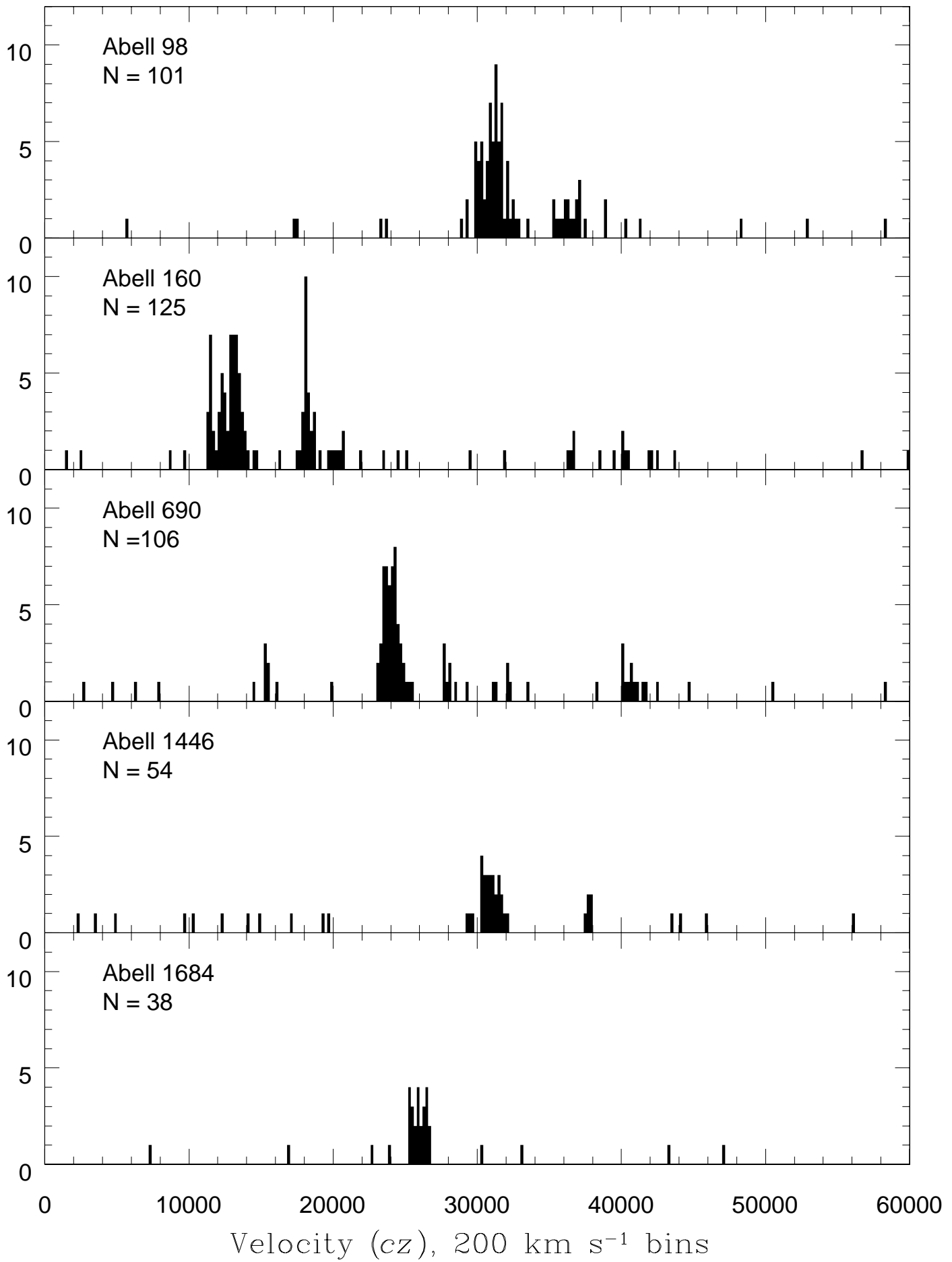
Table 4: Traditional Velocity data for WAT clusters.

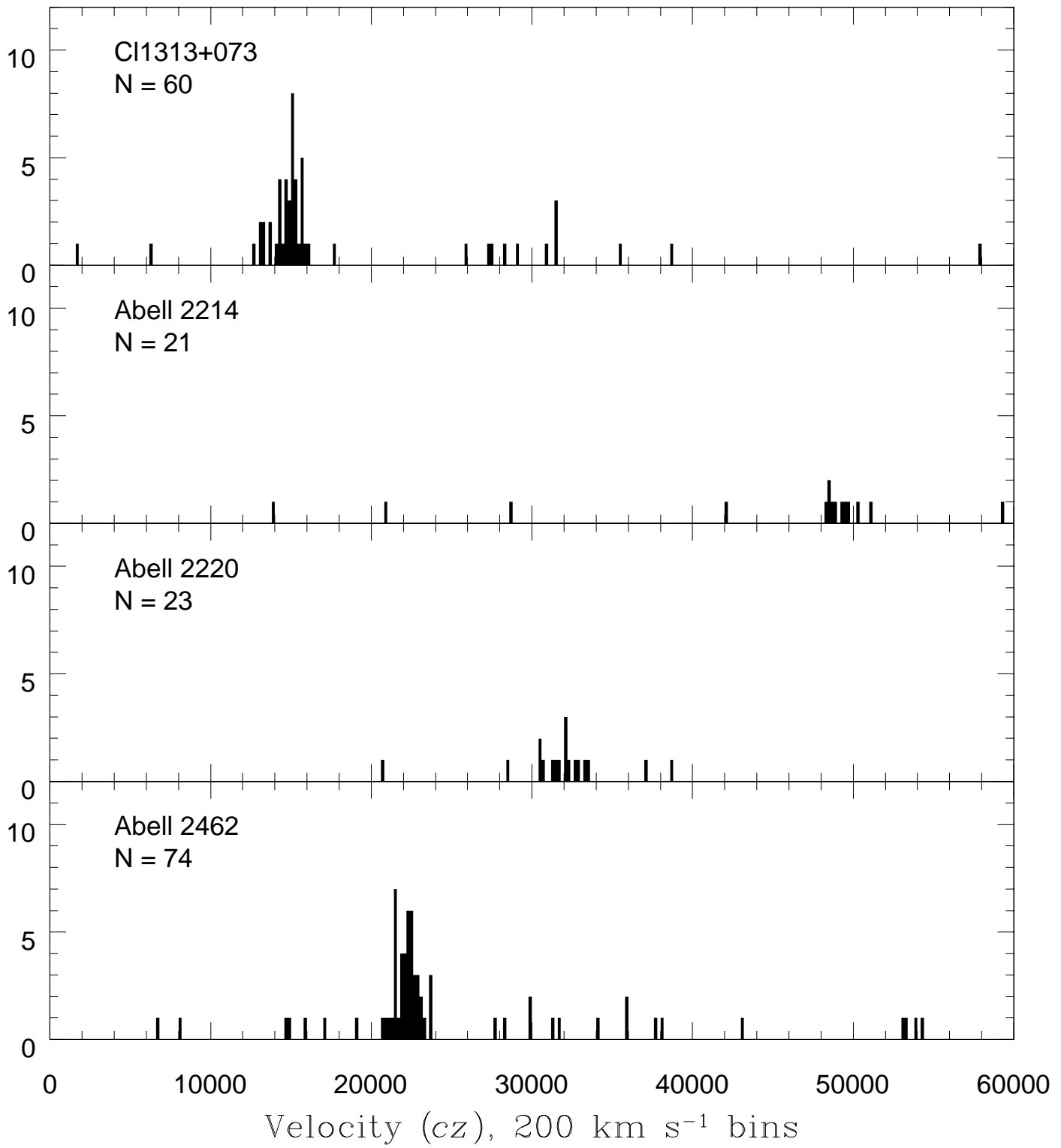
Table 5: Comparison with Published Velocities.

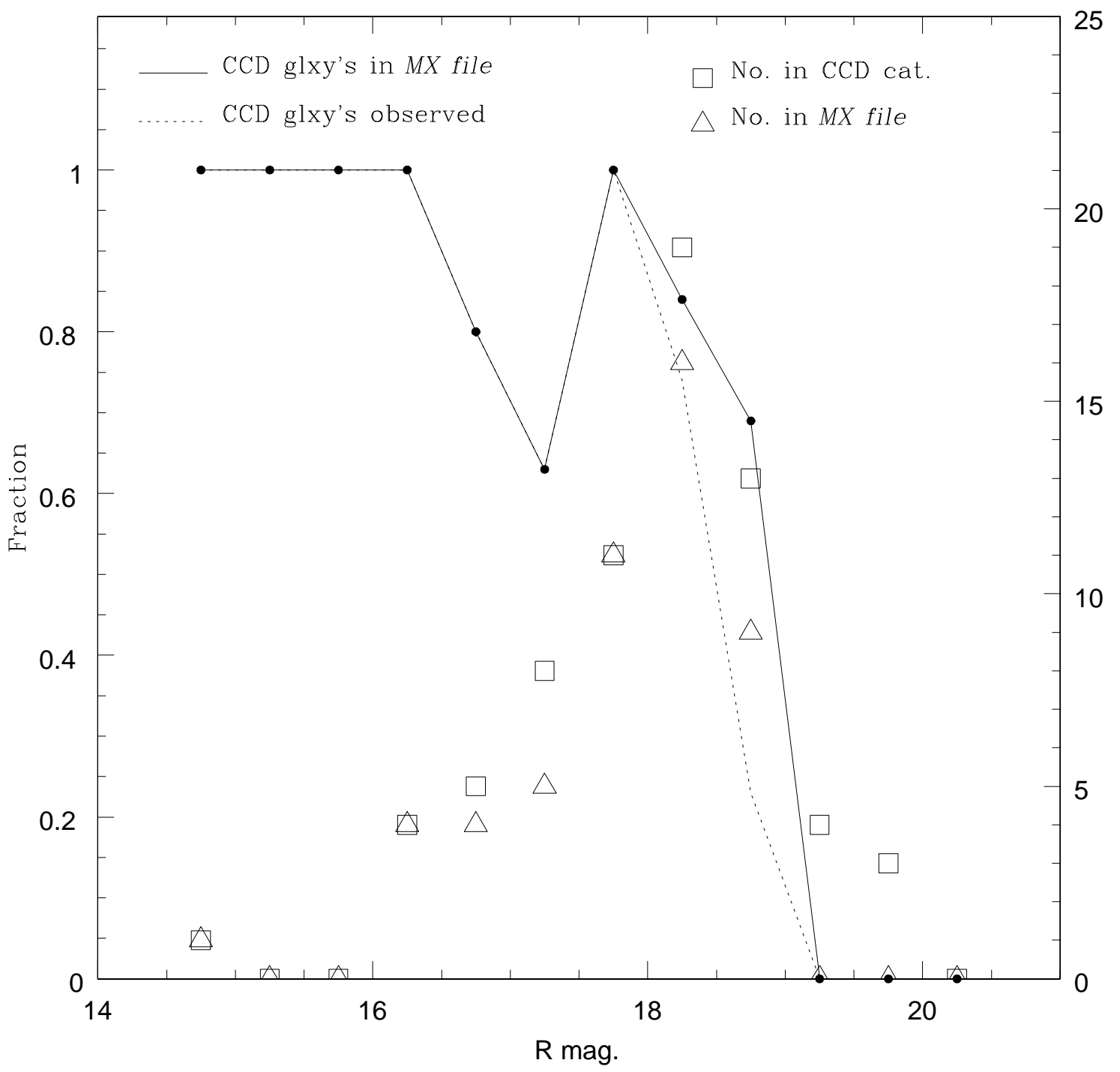
Table 6: Emission Line Galaxy Counts.

Table 7: Spatial Fairness of MX Observations.

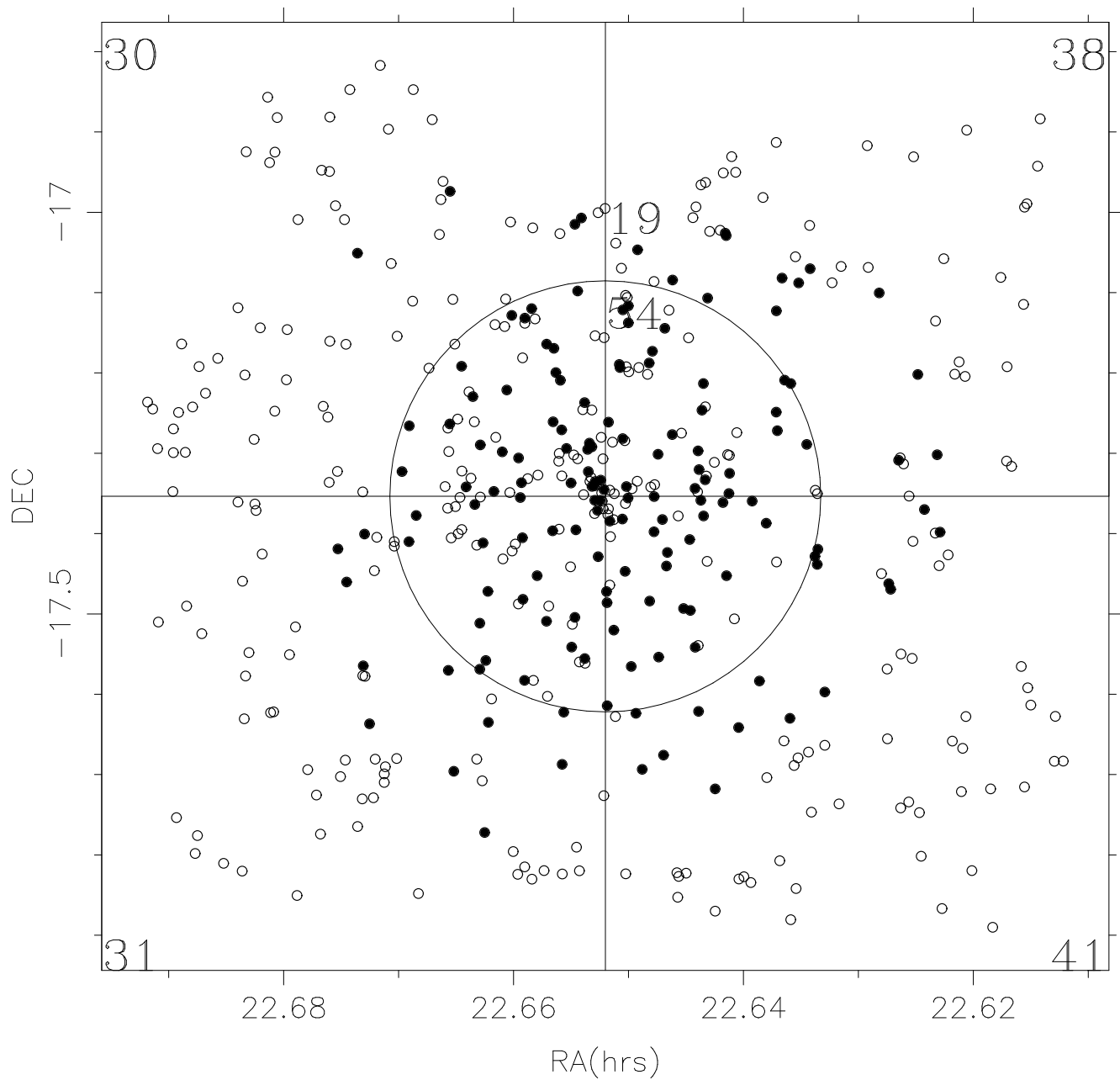








Abell 2462



Abell 690

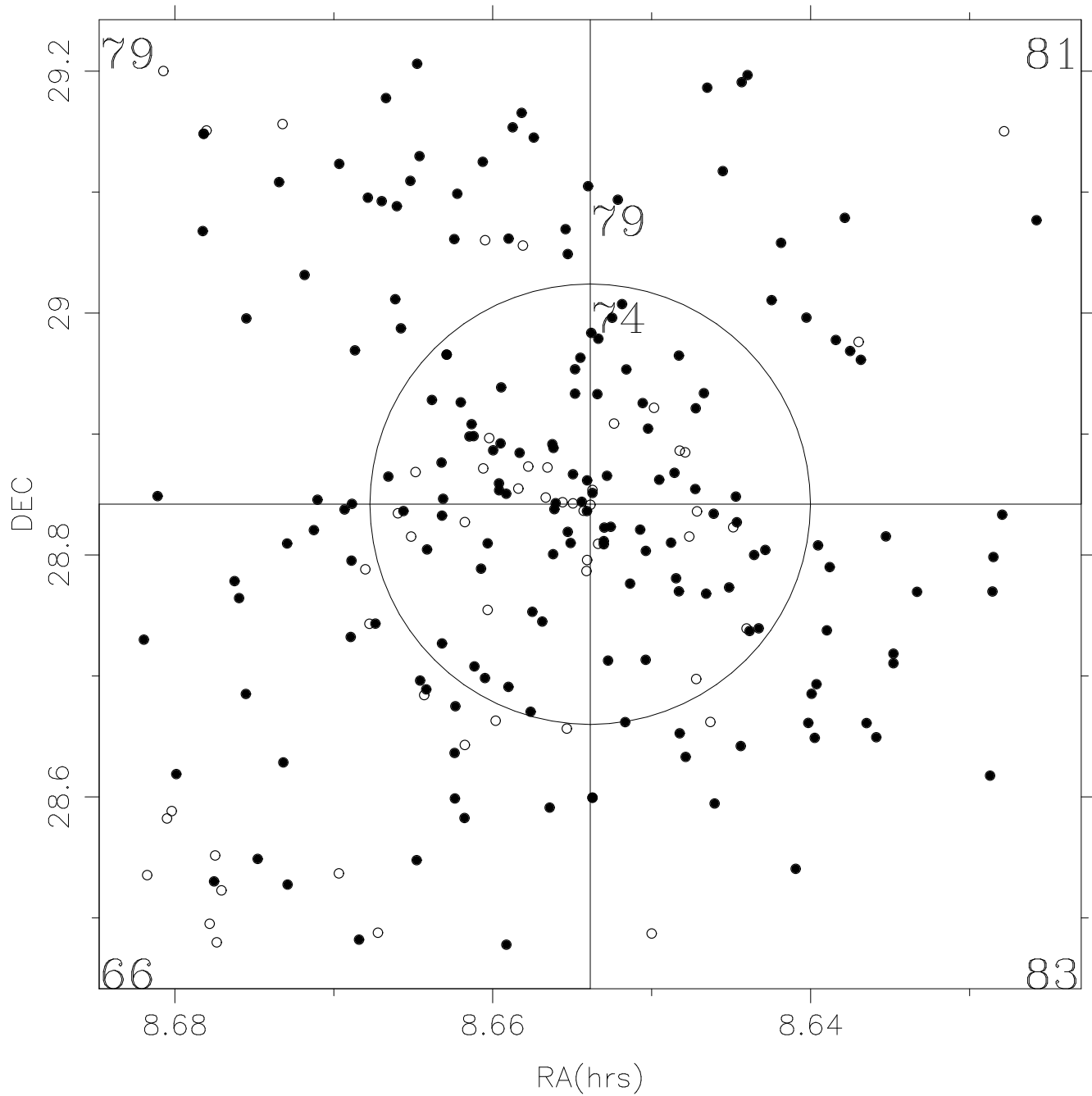


TABLE 1. RADIO PROPERTIES OF WATs

Source	Cluster	Alt.Name	$z^1$	$r/A_C^2$	$\log(P_{1400})^3$	Extent <sup>4</sup>	Morph. <sup>5</sup>	Notes <sup>6</sup>
0043+201	A98	4C20.04	0.1063	0.08	25.12	290	WAT	Z,I,O
0053+261B	A115		0.1971	0.58	25.35	85	WAT?	I
0110+152	A160		0.0440	0.06	24.45	430	TJ	Z,I,O
0255+058A,B	A400	3C75	0.0226	0.08	24.65	330	TJ&TJ	I,P
0803-008	A623		0.0891	0.03	25.31	150	WAT?	P
0836+290	A690	4C29.30	0.0789	0.03	25.12	510	WAT	Z,I,O
1138+060	A1346		0.0972	0.13	24.97	...	WAT?	
1159+583	A1446	4C58.23	0.1025	0.09	25.24	170	WAT	Z,I,P,O
1233+168	A1569		0.0784	0.18	25.23	350	WAT?	P
1306+107	A1684	4C10.35	0.0864	0.28	24.80	460	WAT?	Z,O
1313+073	...		0.0507	...	25.01	300	WAT	Z
1433+553	A1940	4C55.29	0.1402	0.07	25.28	240	WAT	I,P,O
1636+379	A2214	4C37.48	0.1609	0.23	25.55	450	WAT	Z,P,O
1638+538	A2220		0.1103	0.09	25.21	240	WAT	I
1820+689	A2304		0.0881	0.03	25.11	170	WAT?	P
1919+479	...	4C47.51	0.1022	...	25.32	1200	WAT	Z,I,P
2236-176	A2462	PKS2236-17	0.0742	0.06	25.22	200	WAT	Z,P,O
2335+267	A2634	3C465	0.0302	0.04	25.17	320	WAT	I,P

<sup>1</sup>The redshift,  $z$ , is that of the radio galaxy from Owen et al. (1988, 1995).<sup>2</sup>The ratio of the distance of the radio galaxy from the cluster center to the Abell radius.<sup>3</sup>The logarithmic radio power is given in Watts Hz<sup>-1</sup> ( $H_0=75$  km s<sup>-1</sup> Mpc<sup>-1</sup>, and  $q_0=0.0$ ), and is calculated from flux densities given by Owen et al. (1992, 1993) or in OOE.<sup>4</sup>The maximum, projected, linear size of the source (usually between ends of the tails) given in kpc.<sup>5</sup>These morphologies are suggested by Owen from the 20 cm survey (Owen, private communication).<sup>6</sup> Z: New redshifts presented in this paper.I: Observed with *Einstein* IPC.P: Observed with *ROSAT* PSPC.

O: High resolution radio data in O'Donaghue et al (1990, OOE).

TABLE 2. LOG OF MX OBSERVING RUNS

Year	Date	Clusters Observed	Conditions	CCD
1991	Mar 12-13	A690 c1313+073	good	TI 800
1991	Dec 29-30	...	poor - humid	TI 800
1991	Dec 31	A160 A690	good	TI 800
1992	Mar 7	...	poor - blizzard	TI 800
1992	May 31	...	...	CCD out
1992	Aug 26-27	A98 A160 A2462 c1919	poor - clouds	Loral 1
1992	Dec 26 (half)	A98 A160 A690	ok	Loral 2
1992	Dec 27-28	...	poor - clouds	Loral 2
1993	Jan 21-24 (half)	A690 A1446 A1684 c1313	great	Loral 2
1993	Jul 22-23	A160 c1919 A2214 a2462	great	Loral 3
1993	Sep 15-16 (half)	A98 A160 c1919 a2462	good	Loral 3

TABLE 3. VELOCITIES AND POSITIONS OF WAT CLUSTER GALAXIES

Gal. ID	RA(2000)	DEC(2000)	cz1 <sup>a</sup>	cz2 <sup>b</sup>	$\epsilon^c$	NOTES <sup>d</sup>
Abell 98						
201	0 46 35.67	20 29 41.8	31999	...	87	BGH337
202	0 46 29.33	20 28 04.4	30942	...	42	WAT, BGH401
203	0 46 36.26	20 28 26.3	32162	...	44	gE, BGH383
204	0 46 24.63	20 30 07.1	31261	...	45	BGH320?
205	0 46 23.85	20 30 00.0	29895	...	77	BGH328?
212	0 46 19.26	20 28 11.6	30453	...	107	
222	0 46 38.13	20 28 40.8	30981	...	97	
226	0 46 49.17	20 27 24.1	29315	...	95	
227	0 46 49.99	20 27 07.6	31643	...	52	
235	0 46 51.51	20 30 23.3	30547	...	51	
236	0 46 51.79	20 30 42.4	31852	...	51	
237	0 46 48.03	20 30 54.9	31066	...	82	
246	0 46 31.07	20 31 43.7	30991	...	103	
250	0 46 18.52	20 33 13.9	31519	...	75	
251	0 46 15.79	20 32 06.3	30691	...	92	
252	0 46 02.15	20 30 50.4	29872	...	71	
253	0 46 02.24	20 30 30.4	31770	...	79	
256	0 45 41.41	20 30 58.8	30890	...	72	
258	0 45 41.29	20 28 01.8	28811	...	101	
260	0 45 32.12	20 27 23.3	23715	...	103	
261	0 45 45.53	20 26 15.8	31267	...	72	
264	0 46 04.74	20 28 27.5	31612	...	81	
266	0 46 18.80	20 25 57.5	41346	...	96	
267	0 46 22.61	20 25 44.8	48228	...	94	
269	0 46 17.10	20 23 44.1	...	7277	200	
270	0 46 14.69	20 23 41.9	31004	...	48	
271	0 46 28.46	20 23 47.9	30182	...	66	
272	0 46 33.92	20 23 54.6	32705	...	45	
275	0 46 37.02	20 26 06.1	30954	...	90	
279	0 46 38.55	20 22 53.3	31116	...	59	
281	0 46 35.19	20 20 31.0	30701	...	51	
282	0 46 28.17	20 21 05.3	36105	...	96	
283	0 46 33.24	20 14 57.1	35375	...	88	
286	0 46 48.95	20 15 29.4	...	15163	200	
287	0 46 56.82	20 20 35.4	35554	...	48	
288	0 47 01.74	20 23 18.0	em31439	...	59	stO2O3sHs Vab=31413
289	0 46 29.93	20 34 27.5	...	29315	200	
291	0 46 52.58	20 25 23.3	32553	...	100	
295	0 47 09.39	20 29 17.0	31494	...	82	
297	0 47 23.22	20 31 21.5	...	4224	200	
298	0 47 17.58	20 34 54.8	36861	...	91	
299	0 47 12.70	20 35 24.5	52979	...	98	
307	0 46 32.55	20 28 23.8	31766	...	55	
308	0 46 31.99	20 28 27.3	31431	...	87	
315	0 46 36.44	20 15 24.1	36160	...	44	BCG in A98Sb
316	0 46 47.61	20 11 23.4	...	36674	200	
317	0 46 56.04	20 12 23.0	36970	...	60	

TABLE 3. (continued)

Gal. ID	RA(2000)	DEC(2000)	<i>cz1</i> <sup>a</sup>	<i>cz2</i> <sup>b</sup>	$\epsilon^c$	NOTES <sup>d</sup>
318	0 47 05.99	20 17 24.4	38919	...	100	
320	0 47 18.01	20 21 59.9	31451	...	68	
321	0 46 07.49	20 28 48.4	31734	...	77	
324	0 45 45.59	20 18 45.6	23221	...	100	
325	0 45 49.23	20 14 38.7	35977	...	80	
327	0 46 35.27	20 30 11.0	31203	...	52	
336	0 46 26.85	20 36 52.0	29831	...	106	
337	0 46 30.17	20 36 48.7	29380	...	38	BGH142,FD12
340	0 46 20.12	20 35 45.9	40217	...	104	
346	0 46 46.34	20 37 29.2	...	4644	200	
348	0 46 44.64	20 37 00.5	37582	...	98	
351	0 46 45.56	20 40 12.6	40099	...	75	
352	0 46 44.47	20 40 23.9	...	36125	200	
355	0 46 40.72	20 44 04.7	17288	...	97	
358	0 46 32.09	20 43 06.4	31358	...	88	
363	0 46 21.60	20 42 30.3	31354	...	91	
365	0 46 16.64	20 44 12.6	...	6611	200	
368	0 46 07.52	20 40 59.4	...	45628	200	
371	0 45 56.39	20 42 19.2	...	4814	200	
376	0 45 57.44	20 36 55.2	30373	...	75	
378	0 46 07.86	20 38 47.0	31768	...	58	
388	0 46 56.51	20 27 04.8	30250	...	66	
392	0 46 15.51	20 33 19.1	30023	...	48	
393	0 46 18.45	20 32 28.6	58287	...	104	
394	0 46 23.41	20 32 14.5	...	41869	200	
395	0 46 15.58	20 31 00.6	5787	...	102	
397	0 46 08.45	20 28 50.1	30371	...	52	O2,E+A BGH360 FD8
402	0 47 12.97	20 29 41.5	32044	...	59	
403	0 47 06.65	20 23 51.2	36484	...	62	
407	0 46 27.60	20 18 24.2	37169	...	88	
408	0 46 38.51	20 16 20.8	36630	...	50	
413	0 47 25.80	20 10 02.8	37168	...	90	
414	0 46 34.36	20 11 57.4	35692	...	58	
415	0 46 27.67	20 10 41.5	36274	...	70	
416	0 46 20.25	20 08 13.4	35259	...	66	
419	0 46 29.24	20 14 04.6	36398	...	92	
420	0 46 16.29	20 16 12.5	37137	...	83	
421	0 45 59.01	20 15 29.2	38904	...	78	
423	0 45 57.47	20 12 56.0	...	61204	200	
427	0 45 33.02	20 15 07.7	30062	...	54	
428	0 45 40.22	20 15 58.1	29947	...	52	
429	0 45 59.32	20 23 49.6	31713	...	85	
430	0 45 48.57	20 26 05.7	31146	...	50	
431	0 45 50.11	20 29 10.0	30324	...	70	
432	0 45 50.47	20 29 06.7	30966	...	95	
2080	0 46 20.70	20 29 06.0	30947	...	44	
0408	0 46 33.26	20 27 50.4	32456	...	79	BGH408
0396	0 46 31.89	20 28 09.5	32392	...	69	BGH396

TABLE 3. (continued)

Gal. ID	RA(2000)	DEC(2000)	cz1 <sup>a</sup>	cz2 <sup>b</sup>	$\epsilon^c$	NOTES <sup>d</sup>
0411	0 46 25.91	20 27 32.2	31199	...	100	BGH411,FD10
0338	0 46 19.42	20 29 40.2	32855	...	64	BGH338
0311	0 46 16.00	20 30 18.5	31340	...	53	BGH311
0422	0 45 47.03	20 26 55.2	31260	...	38	BGH422
0353	0 46 21.93	20 29 04.8	33446	...	40	BGH353
0354	0 46 20.32	20 28 58.7	30387	...	100	BGH354,FD11
0125	0 46 24.78	20 37 17.3	30741	...	39	BGH125,radio
0067	0 46 29.90	20 38 56.8	32609	...	100	BGH67,FD5
0092	0 46 15.94	20 38 07.7	32124	...	49	BGH92
0158	0 46 43.31	20 36 03.6	31336	...	38	BGH158,FD9
0221	0 46 29.66	20 33 17.0	31330	...	100	BGH221,FD6
0185	0 46 13.69	20 34 50.0	17523	...	100	BGH185,FD4
0184	0 46 04.06	20 34 50.0	30123	...	45	BGH184,FD13
0182	0 45 59.80	20 35 07.8	30772	...	200	BGH182
0175	0 45 52.86	20 35 11.4	10755	...	37	BGH175
0212	0 45 40.67	20 33 38.1	17965	...	68	BGH212
0030	0 46 08.12	20 40 43.3	30612	...	51	BGH30
0042	0 46 52.84	20 41 00.4	31497	...	44	BGH42
0095	0 47 14.01	20 38 09.8	18317	...	80	BGH95
Abell 160						
201	1 12 59.64	15 29 27.4	13172	...	100	TJ
202	1 12 59.94	15 29 29.4	12996	...	80	
203	1 13 03.73	15 30 07.1	12283	...	62	
204	1 12 58.68	15 28 13.9	12846	...	59	
205	1 12 57.66	15 28 19.7	...	3994	200	
207	1 12 49.91	15 30 18.2	12800	...	49	
208	1 12 49.49	15 30 26.1	13596	...	51	
211	1 12 41.17	15 28 21.9	29460	...	99	
212	1 12 38.22	15 28 03.1	12807	...	51	
214	1 12 45.24	15 27 21.5	13234	...	89	
217	1 13 03.93	15 27 16.3	12388	...	65	
218	1 13 05.98	15 26 28.8	24400	...	101	
220	1 13 14.70	15 26 38.5	em13912	...	150	O2O3sHs
222	1 13 07.48	15 27 49.8	13080	...	88	
224	1 13 13.85	15 29 36.9	...	5197	200	
225	1 13 16.28	15 30 09.5	13216	...	54	
226	1 13 15.64	15 30 25.0	14512	...	46	
227	1 13 13.26	15 30 27.3	12056	...	65	
228	1 13 15.73	15 30 58.2	14085	...	20	
229	1 13 07.47	15 30 30.8	13426	...	75	
230	1 13 02.89	15 31 37.5	13707	...	41	
231	1 13 00.16	15 31 50.3	2296	...	103	
233	1 12 54.08	15 32 47.8	13849	...	45	
234	1 12 48.04	15 31 42.2	12367	...	44	
236	1 12 38.04	15 33 02.4	em12852	...	77	O2HsO3N2 Vab=12968
246	1 12 27.43	15 35 27.8	12578	...	111	
247	1 12 25.05	15 38 36.2	13367	...	79	
248	1 12 23.51	15 43 33.6	18281	...	86	

TABLE 3. (continued)

Gal. ID	RA(2000)	DEC(2000)	cz1 <sup>a</sup>	cz2 <sup>b</sup>	$\epsilon^c$	NOTES <sup>d</sup>
249	1 12 35.76	15 43 16.5	em11376	...	55	O2HsO3
250	1 12 43.84	15 42 26.4	11618	...	69	O2O3HsN2 Vem=11615
251	1 12 40.87	15 39 29.9	2530	...	104	
253	1 13 16.50	15 40 35.5	11475	...	86	O2O3HsN2s Vem=11455
254	1 13 19.16	15 42 12.1	12980	...	68	
255	1 13 09.12	15 37 45.4	13441	...	85	
256	1 13 42.32	15 42 02.9	...	69522	200	
257	1 13 45.01	15 40 59.2	13280	...	60	O2HsN2S2 Vem=13221
259	1 13 42.80	15 36 54.1	43762	...	101	
260	1 13 30.95	15 33 04.3	13303	...	71	
261	1 13 30.33	15 32 46.0	12024	...	17	H?
262	1 13 34.51	15 32 24.0	18106	...	60	
264	1 13 40.92	15 31 52.5	...	23621	200	
265	1 13 47.68	15 30 29.0	13561	...	42	
266	1 13 50.61	15 28 18.4	13054	...	20	
267	1 13 47.70	15 26 22.5	40233	...	74	
268	1 13 55.84	15 24 49.3	40134	...	92	
271	1 13 30.26	15 27 02.4	...	22908	200	
272	1 13 16.40	15 23 35.1	13379	...	107	
273	1 13 21.52	15 21 02.8	...	40883	200	
274	1 13 26.71	15 20 06.0	12570	...	68	
276	1 12 30.16	15 16 38.0	...	20387	200	
278	1 12 13.97	15 16 36.8	13583	...	214	
282	1 12 24.47	15 20 07.2	...	12360	200	
283	1 12 24.46	15 21 18.1	13146	...	88	
285	1 12 01.94	15 20 47.0	...	2576	200	
292	1 12 44.03	15 35 20.5	13040	...	87	
293	1 12 53.96	15 36 07.6	12299	...	47	
294	1 12 59.52	15 35 28.6	12348	...	42	O2NeO3N2sHS2 Vem=12200
295	1 13 19.86	15 29 26.3	em14649	...	49	O2O3HsN2 Vab=14858
296	1 12 13.60	15 42 47.4	...	33432	200	
299	1 14 14.51	15 53 52.9	11365	...	65	
302	1 14 02.28	15 48 58.8	11466	...	96	
303	1 14 26.78	15 47 33.1	em11856	...	80	O2O3sHsNe
305	1 14 28.06	15 45 19.3	12559	...	98	
312	1 13 24.70	15 51 21.1	...	44888	200	
313	1 13 21.96	15 51 04.2	13678	...	50	
314	1 13 11.92	15 49 59.2	13209	...	47	
315	1 13 29.98	15 48 56.6	...	29673	200	
316	1 13 24.46	15 46 56.8	11480	...	71	
317	1 13 19.18	15 45 34.2	42490	...	94	
318	1 13 35.60	15 45 28.6	18079	...	94	Hs Vem=17919
320	1 13 45.36	15 47 31.4	...	22566	200	
323	1 12 22.42	15 49 27.6	56704	...	105	
326	1 12 40.79	15 48 52.8	18110	...	98	
327	1 12 42.60	15 49 46.7	...	11127	200	
328	1 12 27.41	15 44 59.0	<sup>6</sup> 11410	...	42	
329	1 12 20.13	15 46 02.4	18104	...	89	

TABLE 3. (continued)

Gal. ID	RA(2000)	DEC(2000)	<i>cz1</i> <sup>a</sup>	<i>cz2</i> <sup>b</sup>	$\epsilon^c$	NOTES <sup>d</sup>
330	1 12 22.35	15 44 19.0	18614	...	66	
331	1 12 29.93	15 44 18.8	11386	...	103	
332	1 12 01.65	15 45 22.8	...	20134	200	
342	1 14 16.86	15 35 32.1	11472	...	60	
343	1 14 09.76	15 35 04.2	17910	...	150	HsN2 Vem=17814
361	1 15 12.57	15 24 37.3	36316	...	100.8	
363	1 15 21.13	15 18 29.2	36720	...	95	
364	1 15 30.75	15 17 15.5	36637	...	40	
366	1 15 08.95	15 17 31.0	20436	...	62	
368	1 14 58.98	15 20 57.9	20081	...	61	
369	1 15 01.19	15 21 20.9	20333	...	69	O2HsO3sO1N2 Vem=20310
370	1 14 35.19	15 20 53.6	...	20405	110	
372	1 14 26.84	15 16 23.9	18428	...	49	
373	1 14 23.11	15 17 17.8	18332	...	46	
375	1 14 22.80	15 23 42.5	40508	...	89	
377	1 14 08.32	15 24 09.4	em17976	...	48	O2O3HsN2S2 Vabs=18308
378	1 14 08.09	15 24 00.9	...	57542	200	
382	1 14 33.50	15 30 09.4	13004	...	100	
383	1 14 35.30	15 30 49.6	em18087	...	40	O2HO3
384	1 14 51.45	15 29 35.0	19849	...	74	
385	1 14 36.45	15 26 25.6	31903	...	102	
387	1 14 53.96	15 41 27.4	...	15555	200	
389	1 14 50.42	15 38 37.1	...	6970	200	
395	1 14 10.18	15 43 28.1	23584	...	99	
396	1 14 07.45	15 43 33.7	em18645	...	51	O2NeHO3s
397	1 14 03.41	15 41 35.2	36418	...	77	
398	1 14 15.75	15 38 11.8	12808	...	48	
400	1 11 52.94	15 41 55.6	18244	...	71	
401	1 11 51.68	15 39 50.9	18069	...	92	
405	1 11 21.99	15 42 25.5	9661	...	99	
415	1 11 24.87	15 34 21.9	18667	...	48	
416	1 11 29.76	15 33 51.9	17871	...	95	
418	1 11 31.31	15 34 16.9	...	2146	200	
420	1 11 48.58	15 34 12.0	1451	...	97	
421	1 11 56.60	15 27 58.2	13149	...	56	
422	1 11 53.33	15 28 10.8	12619	...	90	
425	1 11 50.22	15 21 01.4	17658	...	71	
427	1 11 28.21	15 22 05.4	25183	...	100	
432	1 15 39.52	15 14 42.6	em16395	...	40	O2HsO3N2s
435	1 15 13.45	15 12 45.2	20713	...	64	
438	1 14 22.43	15 14 48.5	18063	...	44	
442	1 14 21.33	15 07 21.9	18336	...	32	
444	1 14 32.34	15 08 28.8	...	21305	200	
445	1 14 17.33	15 03 35.7	18568	...	98	
448	1 14 36.05	14 59 29.4	18127	...	76	
453	1 15 08.42	14 54 02.3	21910	...	89	
462	1 15 20.89	15 02 27.9	38530	...	91	
465	1 14 45.96	15 06 07.6	13175	...	107	

TABLE 3. (continued)

Gal. ID	RA(2000)	DEC(2000)	cz1 <sup>a</sup>	cz2 <sup>b</sup>	$\epsilon^c$	NOTES <sup>d</sup>
468	1 13 26.20	15 15 05.4	12478	...	95	
469	1 13 24.35	15 14 27.2	12672	...	95	
471	1 12 36.45	15 11 47.6	59949	...	103	
473	1 12 28.63	15 11 01.3	42169	...	96	
480	1 12 50.06	15 02 03.5	17458	...	81	
482	1 12 21.90	15 00 37.9	8676	...	87	
484	1 12 20.48	14 58 00.7	11752	...	94	
491	1 13 11.99	15 05 58.0	...	45459	200	
500	1 13 43.04	15 13 52.6	13609	...	74	
502	1 11 21.02	15 12 29.4	...	51237	200	
504	1 11 06.24	15 10 17.7	11457	...	99	HN2 Vem=11520
505	1 11 32.31	15 10 59.1	em12042	...	67	O2O3sHsS2
508	1 11 48.01	15 05 53.1	em11559	...	40	O2O3sHs
511	1 11 36.63	15 04 41.0	41900	...	76	
512	1 11 26.78	15 07 50.2	18078	...	104	
514	1 11 25.92	15 01 02.0	18076	...	44	
515	1 11 50.95	15 03 44.2	em39477	...	52	O2HsO3
516	1 11 46.27	14 58 39.2	13251	...	58	
517	1 11 54.68	14 56 51.3	42398	...	91	
519	1 11 09.81	14 54 10.7	em18073	...	78	O2O3sHsN2
525	1 10 24.06	14 59 11.9	16409	...	50	
531	1 10 37.70	15 06 49.2	...	18012	200	
534	1 11 07.81	15 01 04.8	18303	...	66	O2HsN2s Vem=18394
<hr/>						
Abell 690						
1	8 39 15.83	28 50 38.5	23673	...	75	WAT
2	8 39 14.67	28 50 10.7	24663	...	81	
3	8 39 10.75	28 49 21.4	...	14190	200	
4	8 39 10.85	28 48 31.9	23253	...	79	
5	8 39 19.03	28 49 09.1	40353	...	103	
6	8 39 18.36	28 48 35.9	40115	...	94	
7	8 39 27.05	28 45 11.2	23552	...	107	
10	8 38 47.37	28 46 18.1	24333	...	69	
11	8 38 42.47	28 46 23.7	15370	...	78	
12	8 38 50.13	28 51 16.4	23646	...	96	
13	8 38 58.31	28 51 44.1	14448	...	106	
14	8 38 50.03	28 55 16.5	27623	...	50	
15	8 39 17.37	28 56 00.2	24685	...	82	
16	8 39 17.82	28 52 00.3	24536	...	54	
17	8 39 22.50	28 53 29.8	77610	...	150	
18	8 39 34.59	28 51 33.2	...	27556	200	
19	8 39 32.96	28 51 02.3	23480	...	398	
20	8 39 41.30	28 53 52.8	...	22764	200	
22	8 39 02.61	28 49 15.3	23346	...	63	O2O3s Vem=23349
24	8 39 37.17	28 48 34.9	23833	...	147	
25	8 39 38.66	28 47 19.5	...	25100	200	
28	8 39 24.80	28 44 41.8	24207	...	60	
31	8 39 16.16	28 57 46.8	24296	...	47	
34	8 39 31.49	29 09 12.9	23534	...	78	

TABLE 3. (continued)

Gal. ID	RA(2000)	DEC(2000)	<i>cz1</i> <sup>a</sup>	<i>cz2</i> <sup>b</sup>	$\epsilon$ <sup>c</sup>	NOTES <sup>d</sup>
36	8 39 26.72	29 08 42.1	24097	...	83	
37	8 39 38.27	29 07 30.2	19829	...	99	
38	8 40 10.78	29 07 24.0	23938	...	80	
42	8 39 56.79	28 59 14.7	25202	...	147	
43	8 39 46.42	28 57 56.1	32386	...	98	
44	8 39 58.07	29 00 41.4	42538	...	106	
45	8 40 15.68	28 50 44.4	24280	...	27	
47	8 39 47.61	28 52 35.2	65794	...	132	O2?
48	8 40 18.63	29 01 53.1	64343	...	91	O3s Vem=63684
49	8 40 24.38	29 06 29.9	41654	...	101	
50	8 40 41.69	29 04 04.1	40696	...	84	
53	8 39 04.91	28 46 34.8	23402	...	172	
58	8 38 55.63	28 48 36.7	...	33944	200	
61	8 39 32.45	28 41 27.4	24074	...	148	
62	8 39 37.75	28 41 54.0	24861	...	102	
63	8 39 40.16	28 42 28.3	24105	...	75	
64	8 39 51.05	28 41 19.9	40781	...	79	
65	8 39 47.48	28 43 37.0	23645	...	89	
67	8 40 09.56	28 50 15.6	...	40524	200	
68	8 40 07.90	28 50 32.3	23828	...	270	
69	8 40 23.44	28 37 42.7	24513	...	200	
72	8 40 39.10	28 31 48.5	23892	...	73	
75	8 40 47.68	28 37 08.2	...	25092	200	
76	8 40 31.92	28 41 06.7	50484	...	144	O2?
77	8 40 55.03	28 43 48.2	24723	...	65	
82	8 39 09.28	28 49 24.0	24067	...	32	
83	8 39 08.96	28 59 46.0	...	31311	200	
84	8 38 39.64	29 11 27.0	6245	...	85	
85	8 38 18.32	28 58 39.8	27957	...	100	
88	8 37 43.38	28 37 03.2	15483	...	99	
89	8 38 09.15	28 38 57.6	25194	...	91	
90	8 37 59.92	28 46 10.5	...	36932	200	
91	8 38 22.35	28 48 28.8	40106	...	203	
92	8 38 19.69	28 47 23.8	2669	...	103	
93	8 38 35.77	28 44 22.0	23663	...	49	
95	8 38 22.68	28 41 35.4	15511	...	111	
97	8 38 23.09	28 38 55.9	15382	...	58	
98	8 38 39.84	28 38 31.3	23972	...	54	
99	8 38 27.40	28 32 26.1	...	14776	200	
101	8 39 05.99	28 39 42.5	27782	...	63	
102	8 38 54.84	28 52 04.4	27651	...	104	
103	8 39 14.62	28 51 42.2	23074	...	76	
105	8 39 13.43	28 51 04.7	24052	...	107	
110	8 39 21.77	28 50 34.0	23992	...	101	
111	8 39 22.04	28 50 16.3	23734	...	49	
112	8 39 10.13	28 51 55.9	23635	...	70	
119	8 39 29.91	28 53 03.9	65593	...	117	
121	8 39 34.22	28 53 32.2	4648	...	106	

TABLE 3. (continued)

Gal. ID	RA(2000)	DEC(2000)	<i>cz1</i> <sup>a</sup>	<i>cz2</i> <sup>b</sup>	$\epsilon$ <sup>c</sup>	NOTES <sup>d</sup>
125	8 39 34.10	28 56 19.0	24347	...	104	
126	8 39 46.46	28 57 56.1	32043	...	93	O2HO3 Vem=32025
127	8 39 17.36	28 57 12.8	33469	...	100	
128	8 39 12.30	28 55 58.7	...	12234	200	
129	8 39 05.74	28 57 12.1	41547	...	102	
130	8 38 48.18	28 56 01.4	28124	...	35	
131	8 39 02.03	28 55 32.0	24013	...	91	
135	8 39 47.25	28 50 47.5	38355	...	95	
136	8 39 09.90	28 42 45.9	23348	...	94	
140	8 38 52.33	28 37 59.1	24357	...	53	
141	8 38 24.56	28 39 40.4	16075	...	72	
142	8 38 11.37	28 39 39.8	25422	...	65	O2HO3 Vab=25117
143	8 38 23.78	28 41 07.1	23779	...	78	
145	8 38 37.84	28 44 13.9	24839	...	98	
146	8 38 34.27	28 48 15.3	40091	...	76	
147	8 38 36.82	28 48 00.2	23506	...	116	
149	8 38 40.73	28 49 37.7	24504	...	117	
151	8 38 12.65	28 57 40.9	23448	...	68	
152	8 38 15.08	28 58 07.3	7965	...	107	
154	8 38 24.97	28 59 46.3	28435	...	101	
155	8 38 32.86	29 00 38.5	24198	...	88	
158	8 38 53.84	28 57 53.7	em24950	...	32	O2HO3 Vab=24574
161	8 39 06.72	29 00 26.8	...	54197	200	
163	8 39 32.43	29 03 41.6	24456	...	106	
166	8 39 49.77	28 55 41.5	...	64573	200	
168	8 39 56.22	28 50 10.7	65726	...	51	
170	8 40 16.50	28 49 13.9	23570	...	56	
171	8 40 07.99	28 47 43.3	63229	...	83	
174	8 39 50.89	28 48 16.3	40551	...	129	
177	8 40 08.16	28 43 55.9	...	15010	200	
184	8 39 52.45	28 41 46.1	41073	...	92	
185	8 40 04.29	29 05 43.3	15278	...	12	
186	8 39 54.65	29 06 33.3	em32195	...	81	O2HO3s Vab=32082
187	8 39 44.05	29 05 55.2	24327	...	65	
188	8 39 52.58	29 07 46.9	31357	...	96	
189	8 40 00.17	29 10 39.7	58218	...	93	
190	8 39 53.12	29 12 21.8	24234	...	102	
195	8 40 51.90	28 50 55.3	65840	...	93	
196	8 40 22.58	28 48 34.1	...	61936	200	
408	8 39 42.40	28 34 57.3	23096	...	62	
409	8 39 32.90	28 28 40.5	29208	...	73	
411	8 39 13.41	28 35 57.9	28037	...	102	
414	8 38 43.91	29 07 02.4	40912	...	75	
415	8 38 47.43	29 11 10.9	44790	...	101	
420	8 37 40.62	28 50 00.0	31170	...	95	
421	8 37 42.61	28 47 54.2	24704	...	99	
422	8 37 42.84	28 46 11.2	17457	...	83	
423	8 38 05.26	28 42 37.9	10 <sup>30003</sup>	...	49	

TABLE 3. (continued)

Gal. ID	RA(2000)	DEC(2000)	cz1 <sup>a</sup>	cz2 <sup>b</sup>	$\epsilon^c$	NOTES <sup>d</sup>
424	8 38 45.76	28 35 40.4	24270	...	90	
425	8 39 13.41	28 35 57.9	27927	...	106	
Abell 1446						
201	12 2 03.68	58 02 07.1	30826	...	41	WAT
212	12 2 06.51	58 05 12.4	3542	...	91	
215	12 1 54.72	58 01 40.0	31026	...	104	
221	12 1 49.99	58 00 04.7	31233	...	90	
222	12 1 40.26	58 00 00.1	31641	...	98	
237	12 2 09.28	58 00 20.7	31577	...	63	
238	12 2 09.60	57 59 46.9	em30317	...	47	O2HO3s
243	12 2 15.66	58 00 40.8	29326	...	95	
246	12 2 21.95	58 04 41.9	...	11247	200	
251	12 1 55.70	57 58 15.3	30378	...	53	
252	12 1 16.03	57 59 00.2	em32176	...	125	O2HO3s
254	12 1 46.58	57 57 02.3	...	65236	200	
255	12 1 41.60	57 57 05.6	...	12087	200	
259	12 2 00.40	57 55 39.7	17154	...	93	
260	12 2 13.29	57 57 10.9	30245	...	42	
266	12 2 30.87	57 55 11.1	30421	...	80	
268	12 2 13.52	57 53 31.1	61342	...	93	
270	12 1 40.12	57 52 46.6	37775	...	85	
271	12 1 38.44	57 52 32.4	31012	...	89	
275	12 0 28.86	57 52 10.9	45833	...	88	
276	12 0 37.97	57 53 37.2	30614	...	90	
283	12 0 15.74	57 59 38.7	30411	...	50	
289	12 1 06.14	58 00 10.6	30944	...	28	
291	12 1 30.74	58 02 01.0	30880	...	72	
292	12 1 28.46	58 02 48.8	19354	...	64	
293	12 1 24.73	58 03 23.3	4956	...	99	
294	12 1 30.77	58 03 26.4	em30321	...	74	O2NeHO3
295	12 1 21.52	58 04 18.3	19642	...	52	
302	12 0 21.22	58 03 59.8	...	31808	200	
305	12 0 35.60	58 07 48.5	em10296	...	89	O2HsO3N2
306	12 0 56.18	58 06 51.3	56182	...	90	
314	12 0 29.86	58 10 39.1	37983	...	73	
316	12 1 02.68	58 09 48.7	31110	...	100	
318	12 1 02.08	58 14 05.8	29603	...	88	
319	12 1 23.98	58 10 28.1	37782	...	94	
320	12 1 26.39	58 12 9.8	43565	...	80	
322	12 1 30.47	58 13 13.3	29513	...	103	
323	12 1 44.52	58 12 49.7	em9774	...	70	O2O3HN2
326	12 1 38.28	58 07 25.4	44162	...	99	
329	12 1 46.97	58 07 11.2	12371	...	34	
330	12 1 49.78	58 05 53.5	em12330	...	40	stO2O3sH
332	12 2 01.25	58 06 00.4	31573	...	66	
338	12 3 30.95	58 15 23.6	em14834	...	46	O2HsO3s
340	12 3 26.60	58 11 33.7	37960	...	100	
345	12 2 58.85	58 12 56.0	37487	...	61	

TABLE 3. (continued)

Gal. ID	RA(2000)	DEC(2000)	cz1 <sup>a</sup>	cz2 <sup>b</sup>	$\epsilon^c$	NOTES <sup>d</sup>
353	12 1 55.90	58 11 10.7	30597	...	100	
354	12 2 21.67	58 07 05.8	...	30962	200	
358	12 3 02.43	58 07 01.3	19774	...	90	
365	12 3 32.48	58 04 17.0	31736	...	84	
366	12 3 27.12	58 02 26.4	31260	...	83	
367	12 3 15.97	58 03 10.4	2288	...	94	
369	12 2 39.08	58 03 40.2	31476	...	47	O2O3 Vem=31655
372	12 2 39.54	58 01 18.7	30682	...	56	
373	12 2 41.22	58 00 43.7	30755	...	45	
374	12 3 06.12	58 00 43.3	31977	...	93	
376	12 3 45.62	57 59 22.3	31062	...	107	
380	12 3 20.68	57 55 15.8	31183	...	135	
383	12 3 13.37	57 53 53.2	em10230	...	64	stO2HO3sHsO1N2 Vab=10127
384	12 3 11.55	57 53 36.1	...	23941	200	
385	12 3 13.83	57 53 23.4	em10209	...	70	stO2NeHsO3sN2 Vab=10352
387	12 3 04.25	57 53 15.8	...	37104	200	
390	12 2 55.72	57 51 58.7	30827	...	56	
Abell 1684						
1	13 9 04.47	10 29 35.0	25961	...	38	WAT
3	13 8 59.02	10 29 31.4	25993	...	51	
5	13 9 02.73	10 30 16.5	26445	...	65	
9	13 9 07.68	10 30 07.2	...	47346	200	
10	13 9 07.79	10 29 54.8	25522	...	44	
11	13 9 11.47	10 27 50.7	25982	...	68	
13	13 8 53.05	10 28 26.5	26227	...	90	
15	13 8 56.83	10 30 42.8	26388	...	75	
17	13 8 54.79	10 31 14.3	25346	...	30	gE
23	13 9 05.67	10 36 10.7	25222	...	172	
24	13 9 10.85	10 37 01.5	26160	...	147	gE
25	13 9 22.07	10 35 18.7	26634	...	89	
26	13 9 31.67	10 36 00.3	26412	...	71	
29	13 9 18.83	10 31 52.6	30340	...	76	
31	13 9 32.80	10 28 11.3	25336	...	74	
32	13 9 21.32	10 26 57.7	47004	...	61	
34	13 9 18.86	10 24 29.6	25767	...	43	
35	13 9 13.81	10 23 29.5	16811	...	85	O2HO3s Vem=16859
39	13 8 44.75	10 27 32.0	26140	...	81	
41	13 8 43.09	10 30 05.5	25260	...	135	
43	13 8 29.07	10 30 57.3	33070	...	106	
45	13 8 08.99	10 34 40.3	...	46932	200	
46	13 8 31.28	10 33 19.2	...	47324	200	
47	13 8 31.02	10 35 35.7	26269	...	86	
50	13 8 28.61	10 40 08.1	7329	...	35	O2HsO3sN2 Vem=7339
52	13 9 09.86	10 37 17.9	26400	...	94	
54	13 9 17.69	10 40 24.7	...	9555	200	
55	13 9 30.55	10 42 10.2	25551	...	42	
56	13 9 42.35	10 43 18.1	12 26781	...	64	
59	13 9 34.75	10 33 12.9	26432	...	20	

TABLE 3. (continued)

Gal. ID	RA(2000)	DEC(2000)	cz1 <sup>a</sup>	cz2 <sup>b</sup>	$\epsilon^c$	NOTES <sup>d</sup>
61	13 9 44.50	10 32 01.0	25663	...	27	
64	13 9 35.09	10 30 15.1	22625	...	51	O2HsO3s Vem=22596
65	13 9 55.26	10 29 39.2	...	25993	200	
66	13 9 34.67	10 26 16.2	43373	...	215	
67	13 9 38.46	10 24 48.6	23966	...	101	
74	13 8 45.85	10 20 41.1	25985	...	78	
76	13 8 29.43	10 19 28.8	25557	...	75	
77	13 8 31.71	10 17 12.9	em70490	...	30	O2HsO3s
78	13 8 12.61	10 16 45.1	25812	...	61	
79	13 8 09.51	10 16 38.0	16598	...	90	
80	13 8 34.03	10 25 04.9	25660	...	67	
81	13 8 20.05	10 25 28.6	66440	...	72	
82	13 8 10.83	10 25 40.9	26037	...	87	
1313+073						
1	13 16 17.02	7 02 46.6	15086	...	76	WAT
2	13 16 21.16	6 59 38.5	14682	...	68	
3	13 16 03.35	7 04 50.7	6233	...	98	
5	13 16 12.92	7 01 28.5	25966	...	81	
6	13 16 15.24	7 03 03.4	15309	...	96	
7	13 16 12.68	7 01 48.4	...	13766	200	
8	13 16 15.20	7 02 24.0	15043	...	45	
11	13 16 10.44	6 58 42.0	...	10722	200	
12	13 16 07.78	6 58 32.3	14595	...	124	
13	13 16 01.25	7 01 15.8	16059	...	124	
14	13 16 19.69	6 56 22.2	...	24436	200	
16	13 16 36.87	7 00 54.5	14269	...	63	
17	13 16 32.42	7 01 58.4	15607	...	89	
19	13 16 36.50	7 05 03.3	14777	...	78	
20	13 16 40.98	7 06 13.4	14159	...	106	
21	13 16 34.84	7 07 15.4	15232	...	79	
22	13 15 56.41	7 05 46.7	14336	...	80	
23	13 16 30.92	7 03 17.8	38630	...	104	
24	13 15 03.74	7 17 45.5	31586	...	74	
25	13 15 08.27	6 55 22.1	15695	...	142	
26	13 15 16.44	6 50 14.8	15536	...	72	
27	13 15 26.48	6 48 54.2	...	19885	200	
29	13 15 33.38	6 42 19.1	27395	...	88	
32	13 15 00.39	6 52 15.6	...	3082	200	
33	13 14 58.66	6 47 38.2	15719	...	95	
35	13 15 09.41	6 41 50.4	31524	...	90	
36	13 15 10.17	7 19 34.3	...	16497	200	
37	13 15 19.90	7 19 05.5	13010	...	139	
42	13 14 53.52	7 14 19.6	13109	...	69	
43	13 16 16.97	7 02 57.5	14952	...	40	
45	13 16 10.07	7 02 36.9	14708	...	62	
48	13 16 17.03	6 37 52.3	14864	...	90	
49	13 17 03.83	6 42 41.9	1788	...	101	
50	13 17 22.17	6 50 31.7	15397	...	56	

TABLE 3. (continued)

Gal. ID	RA(2000)	DEC(2000)	cz1 <sup>a</sup>	cz2 <sup>b</sup>	$\epsilon^c$	NOTES <sup>d</sup>
51	13 17 46.75	6 36 55.8	...	8784	200	
54	13 17 25.28	6 52 51.9	17757	...	99	
55	13 17 18.14	7 02 20.7	15689	...	72	
62	13 17 52.86	6 49 45.8	35584	...	104	
65	13 16 52.39	7 17 23.7	14768	...	62	
66	13 16 36.40	7 18 33.9	30808	...	101	
70	13 16 57.72	7 13 09.3	12790	...	66	O2HO3 Vem=12762
71	13 17 02.43	7 09 58.2	14321	...	40	
72	13 17 31.93	7 10 30.1	...	30141	200	
73	13 17 36.00	7 18 01.5	em13680	...	54	O2HO3s
74	13 18 06.38	7 07 38.0	14976	...	57	HO3s Vem=14907
76	13 16 27.62	7 02 06.0	15118	...	73	
80	13 16 16.02	7 06 50.0	15044	...	52	
83	13 16 36.97	7 05 09.4	14360	...	43	
86	13 16 03.34	6 56 29.9	15958	...	74	
87	13 16 11.51	7 00 12.3	15082	...	57	
92	13 15 46.54	6 59 48.2	57810	...	98	
95	13 15 08.64	6 58 37.0	15185	...	100	
100	13 15 24.69	6 54 43.7	...	20578	200	
102	13 15 53.05	6 51 00.2	29065	...	75	
103	13 15 55.54	6 55 43.8	...	5894	200	
104	13 15 53.68	6 42 14.3	15659	...	99	
106	13 16 17.03	6 37 52.3	15093	...	39	
107	13 15 26.74	6 35 32.4	...	24280	200	
110	13 15 57.02	7 17 02.9	em13206	...	64	O2NeHO3s
112	13 14 56.46	7 04 11.5	13627	...	82	
113	13 16 08.27	7 26 30.7	13380	...	66	
114	13 15 26.20	7 25 02.1	31481	...	79	
116	13 15 03.11	7 29 06.1	27480	...	102	
121	13 14 28.34	7 29 34.3	28253	...	96	
122	13 16 00.49	6 47 19.3	15393	...	63	
130	13 15 53.58	6 41 05.0	15068	...	77	
131	13 16 05.47	6 35 47.1	...	41361	200	
132	13 14 55.62	6 40 50.3	27785	...	65	
135	13 14 59.45	6 43 50.8	27400	...	99	
141	13 15 57.88	7 19 47.3	13512	...	102	
145	13 15 11.84	7 07 53.8	41465	...	103	
172	13 16 50.18	7 05 33.8	em11958	...	67	O2HsO3sN2
190	13 16 30.11	7 16 04.4	...	7500	200	
Abell 2214						
1	16 38 00.80	37 52 59.0	48526	...	67	WAT
2	16 38 04.60	37 53 09.8	48626	...	89	
4	16 38 05.38	37 52 09.5	49210	...	92	
9	16 37 58.17	37 53 29.4	49453	...	85	
10	16 37 59.10	37 53 44.0	48278	...	46	
23	16 38 19.44	37 53 14.0	49634	...	67	
25	16 38 30.02	37 53 19.1	48884	...	85	
26	16 38 16.36	37 52 19.7	66273	...	93	

TABLE 3. (continued)

Gal. ID	RA(2000)	DEC(2000)	cz1 <sup>a</sup>	cz2 <sup>b</sup>	$\epsilon^c$	NOTES <sup>d</sup>
40	16 37 23.34	37 47 25.1	28788	...	96	
46	16 37 26.01	37 53 12.8	50208	...	74	
47	16 37 26.65	37 53 17.3	20871	...	99	
82	16 39 04.32	37 53 17.6	48514	...	99	
84	16 39 12.50	37 50 54.8	13983	...	102	
91	16 37 51.84	37 44 40.5	42029	...	88	
92	16 37 44.83	37 45 18.1	59317	...	91	
109	16 37 18.20	37 51 46.5	51109	...	66	
111	16 37 20.44	37 53 13.5	48623	...	73	
118	16 36 49.69	37 57 14.9	48510	...	91	
120	16 37 02.79	38 00 59.9	49631	...	103	
131	16 38 10.23	38 01 17.4	18725	...	103	
132	16 38 04.80	38 05 20.8	18552	...	75	
Abell 2220						
206	16 41 22.53	54 00 15.9	32081	...	81	
207	16 40 54.90	53 54 35.5	32791	...	86	
210	16 39 52.02	53 47 39.6	32083	...	56	gE
211	16 40 12.10	53 45 10.9	31479	...	60	
214	16 39 47.56	53 47 27.8	33392	...	83	
216	16 37 45.80	53 49 23.4	31691	...	78	
217	16 37 11.04	53 47 49.8	...	22055	200	
218	16 37 42.11	53 47 29.5	30506	...	65	
220	16 38 33.30	53 46 22.2	30682	...	94	
224	16 37 45.94	53 50 43.5	32026	...	105	
225	16 38 52.69	53 55 56.4	30406	...	74	
226	16 39 32.63	53 46 43.6	32991	...	63	WAT
228	16 39 19.57	53 47 43.5	32261	...	66	
229	16 39 25.76	53 45 45.1	37045	...	89	
230	16 39 34.80	53 48 42.9	33466	...	63	
233	16 38 50.21	53 53 13.1	...	43979	200	
234	16 38 14.68	54 01 48.0	38751	...	97	
239	16 39 13.61	54 00 45.2	31354	...	96	
246	16 39 20.28	54 06 35.3	28453	...	88	
247	16 38 03.65	54 04 49.9	20638	...	43	
250	16 40 55.59	53 31 26.0	...	14685	200	
272	16 38 46.49	53 35 34.4	32723	...	46	
287	16 38 36.95	53 43 38.1	32430	...	82	
292	16 39 37.37	53 45 36.3	32574	...	105	
293	16 39 54.43	53 44 55.9	36964	...	80	
294	16 39 52.95	53 44 00.4	31717	...	87	
Abell 2462 (= A3897)						
1	22 39 11.42	-17 20 28.7	22233	...	39	WAT, enacs8
2	22 39 10.72	-17 20 26.1	22078	...	96	
4	22 39 10.42	-17 20 06.9	64660	...	104	
5	22 39 08.72	-17 20 00.5	23631	...	83	
7	22 39 12.57	-17 19 21.6	22210	...	56	
13	22 39 10.55	-17 21 30.7	22971	...	86	
14	22 39 09.73	-17 22 15.3	21610	...	47	enacs7

TABLE 3. (continued)

Gal. ID	RA(2000)	DEC(2000)	<i>cz1</i> <sup>a</sup>	<i>cz2</i> <sup>b</sup>	$\epsilon$ <sup>c</sup>	NOTES <sup>d</sup>
20	22 39 17.98	-17 20 13.0	21944	...	54	
24	22 39 19.41	-17 17 38.5	...	21051	200	
27	22 39 12.25	-17 17 14.6	22543	...	41	
28	22 39 11.45	-17 17 31.5	21465	...	64	
29	22 39 12.81	-17 17 42.9	21304	...	35	
36	22 39 00.64	-17 20 29.3	35868	...	75	
38	22 38 51.97	-17 21 14.4	22428	...	52	
41	22 39 01.90	-17 22 54.9	...	4159	200	
43	22 39 05.88	-17 23 04.0	21471	...	45	enacs5
48	22 38 52.01	-17 23 51.8	35969	...	90	
50	22 38 48.13	-17 26 25.2	14715	...	66	enacs3
51	22 38 29.33	-17 27 08.9	21448	...	84	enacs1, O3sHN2 Vem=21384
53	22 38 40.65	-17 29 44.7	...	10200	200	
57	22 38 53.38	-17 29 02.6	37652	...	88	
58	22 39 01.06	-17 26 49.0	22044	...	89	
59	22 39 09.53	-17 25 43.7	21492	...	40	
61	22 39 06.86	-17 28 19.8	21592	...	98	
62	22 39 06.70	-17 29 09.9	29873	...	79	
63	22 39 04.61	-17 31 12.8	53126	...	96	
64	22 39 16.78	-17 30 15.3	22419	...	48	
66	22 39 25.70	-17 30 33.2	29997	...	87	enacs11
72	22 39 46.57	-17 30 41.6	...	em21792	200	wkO2HO3
77	22 39 33.21	-17 24 18.7	62337	...	74	
78	22 39 45.55	-17 24 42.1	22227	...	97	
80	22 39 55.51	-17 24 19.6	14934	...	80	enacs12
83	22 39 23.75	-17 23 47.6	23607	...	67	
88	22 39 33.54	-17 20 11.6	21966	...	75	
89	22 39 33.86	-17 21 18.4	53960	...	96	
91	22 39 42.17	-17 20 50.6	23360	...	66	
93	22 39 48.15	-17 21 49.5	23108	...	76	
101	22 39 34.43	-17 18 20.9	22156	...	44	
102	22 39 39.52	-17 17 53.8	...	17025	200	
112	22 39 52.27	-17 11 29.8	54267	...	68	
114	22 39 38.10	-17 13 16.6	15802	...	102	
115	22 39 25.63	-17 09 50.8	22676	...	91	
117	22 39 22.73	-17 11 58.0	...	1375	200	
118	22 39 21.34	-17 12 33.1	21469	...	46	enacs10
119	22 39 23.61	-17 15 39.3	...	63998	200	
120	22 39 20.93	-17 16 15.5	21442	...	102	
126	22 39 06.26	-17 15 40.7	22345	...	62	
130	22 39 02.69	-17 11 35.7	38023	...	77	
135	22 38 53.55	-17 11 15.6	22719	...	47	enacs4
144	22 38 46.32	-17 16 36.1	22677	...	80	O2?
152	22 38 35.99	-17 19 58.6	21955	...	62	enacs2
156	22 38 30.43	-17 21 41.0	...	8648	200	
157	22 38 37.37	-17 21 30.8	...	38083	200	
158	22 38 36.49	-17 22 40.7	...	23178	200	
163	22 38 04.21	-17 17 20.5	...	8386	200	

TABLE 3. (continued)

Gal. ID	RA(2000)	DEC(2000)	cz1 <sup>a</sup>	cz2 <sup>b</sup>	$\epsilon^c$	NOTES <sup>d</sup>
164	22 38 21.25	-17 21 34.6	...	7635	200	
167	22 38 16.90	-17 23 13.7	23763	...	99	
169	22 38 00.70	-17 25 10.4	...	34728	200	
173	22 37 38.48	-17 27 44.3	6683	...	89	
174	22 37 37.92	-17 28 09.8	27706	...	72	
178	22 37 22.43	-17 23 53.6	21012	...	84	
180	22 37 27.31	-17 22 11.8	20700	...	56	
192	22 37 23.32	-17 18 06.3	...	24089	200	
194	22 38 39.10	-17 32 29.3	em20808	...	74	O2NeHs
196	22 38 59.14	-17 33 55.6	17001	...	101	
197	22 39 17.78	-17 32 28.8	...	22133	200	
401	22 39 56.42	-17 34 12.6	8077	...	106	
404	22 39 32.55	-17 34 58.0	31353	...	81	
409	22 39 20.29	-17 37 20.2	22361	...	62	enacs9
410	22 39 06.69	-17 36 51.2	23161	...	81	enacs6
414	22 38 25.52	-17 38 29.1	em22012	...	63	O2O3O1H
416	22 38 55.69	-17 41 36.4	...	30760	200	
439	22 38 32.87	-17 43 04.1	43023	...	97	
462	22 40 08.65	-17 15 56.7	28388	...	72	
463	22 40 10.91	-17 19 22.0	22424	...	84	
467	22 40 06.46	-17 22 38.6	22879	...	68	
468	22 40 22.67	-17 24 01.9	22952	...	74	
471	22 40 08.74	-17 24 36.2	22497	...	83	enacs13
473	22 40 30.99	-17 25 08.5	53217	...	68	
475	22 40 28.28	-17 27 36.9	22590	...	90	
488	22 39 36.56	-17 07 42.2	22343	...	56	
489	22 39 32.44	-17 07 54.2	21858	...	42	
490	22 39 30.33	-17 07 11.5	...	em23385	200	wkO1N2HS2
496	22 39 55.85	-16 58 26.2	19053	...	107	
500	22 39 14.78	-17 00 25.7	...	23151	200	
504	22 38 57.15	-17 02 47.9	31769	...	96	
506	22 39 15.90	-17 05 52.8	...	21481	200	
510	22 39 00.07	-17 06 59.5	34177	...	107	
516	22 38 48.60	-17 08 40.2	22060	...	81	
517	22 38 35.25	-17 06 24.8	...	10193	200	
565	22 38 11.91	-17 04 54.9	22550	...	75	
571	22 37 41.49	-17 06 01.1	27969	...	104	
586	22 40 21.07	-17 38 12.5	22460	...	53	
608	22 37 58.50	-17 35 49.7	41243	...	94	

<sup>a</sup>Category 1 heliocentric velocity in km s<sup>-1</sup>. Velocities beginning in "em" are measured from emission lines.<sup>b</sup>Category 2 heliocentric velocity in km s<sup>-1</sup>.<sup>c</sup>Velocity error in km s<sup>-1</sup>, see text.<sup>d</sup>Key to NOTES: WAT - wide-angle tailed radio galaxy; TJ - Twin Jet morphology; FD - id from Faber & Dressler 1977; BGH - id from Beers, Geller, & Huchra 1982; gE - giant elliptical, usually 2nd ranked in cluster.

The following codes pertain to the emission line survey: H = hydrogen Balmer line; O3 = [OIII] 4363, 4959 or 5007Å; O2 = [OII] 3727Å; O1 = [OI] 6300Å; N1 = [NI] 5199Å; N2 = [NII] 6548 or 6583Å; Ne = [NeIII] 3869Å; E+A = strong H absorption blueward of Ca lines ; s = pluralizes the preceding code to refer to 2 or more lines from a species; em = emission; ab = absorption; st = strong; wk = weak; ? = uncertain. Absorption line velocities are placed in the notes column if they are significantly less certain than the emission line velocity.

TABLE 4. TRADITIONAL VELOCITY DATA FOR WAT CLUSTERS

Cluster Name	$N_{tot}$	$N_{Memb}$	$V_\mu$ km s $^{-1}$	$S_\sigma$ km s $^{-1}$
A98(N+S)	101	69	31,085 $\pm$ 96	797 $\pm$ 73
A160	125	65	12,814 $\pm$ 102	1062 $\pm$ 144
A690	106	57	24,109 $\pm$ 69	950 $\pm$ 217
A1446	54	31	30,865 $\pm$ 112	616 $\pm$ 83
A1684	38	29	25,791 $\pm$ 79	760 $\pm$ 246
Cl1313+073	60	43	14,742 $\pm$ 128	999 $\pm$ 142
A2214	21	13	49,139 $\pm$ 156	706 $\pm$ 197
A2220	23	19	32,274 $\pm$ 199	1297 $\pm$ 488
A2462	74	48	22,172 $\pm$ 97	784 $\pm$ 133

Notes to Table 4.

$V_\mu$  is the mean of the velocities within 4000 km s $^{-1}$  of the WAT velocity. There is no clipping or correction for substructure in these velocity samples.  $S_\sigma$  is the velocity dispersion as estimated by the standard deviation with a cosmological correction factor of  $(1+z)^{-1}$ .

TABLE 5. COMPARISON OF GALAXY VELOCITIES

Galaxy ID	$cz_{us}$ km s $^{-1}$	$cz_{ref}$ km s $^{-1}$	$\Delta cz$ km s $^{-1}$	References
A98 203	32162±44	32041±48	121	1
		32070±51	92	2
A98 202	30942±42	30989±40	-47	1
		31001±46	-59	2
A98 201	32000±88	32164±202	-164	1
		31710±91	290	2
A98 204	31262±45	31351±54	-89	1
		31367±55	-105	2
A98 205	29895±78	29860±53	35	1
		29910±54	-15	2
A98 397	30371±53	30565±100	-193	3
A98 337	29380±38	29512±100	-132	3
A2462 50	14715±67	14746±54	31	4
A2462 66	29998±88	29817±81	-181	4
A2462 51	21449±85	21414±78	-35	4
A2462 152	21955±62	21988±57	33	4
A2462 135	22720±48	22369±87	-351	4
A2462 43	21471±45	21311±75	-160	4
A2462 410	23162±82	23147±60	-15	4
A2462 14	21610±48	21578±63	-32	4
A2462 1	22234±39	22198±57	-36	4
A2462 409	22361±62	22208±60	-153	4
A2462 118	21469±47	21350±63	-119	4
A2462 471	22498±83	22330±63	-168	4

References for Table 5.

(1) Beers, Geller & Huchra 1982 (BGH), (2) Zabludoff, Huchra, & Geller 1990, (3) Faber & Dressler 1977, (4) Katgert, Mazure, den Hartog, Adami, Biviano, & Perea (1998).

TABLE 6. EMISSION LINE GALAXY COUNTS

Cluster	z <sup>1</sup>	Members <sup>2</sup>	%ELGs <sup>3</sup>	%ELGs Non-mem <sup>4</sup>	H $\alpha$ <sup>5</sup>	Comments <sup>6</sup>
Abell 98	0.1037	53 <sup>a</sup>	1.9(1/53)	0.0(0/28)	7261Å	NS interferes w/OIII
Abell 160	0.0427	65	20.0(13/65)	15.0(9/60)	6852Å	NS interferes w/H $\beta$
Abell 690	0.0804	56	5.4(3/56)	6.0(3/50)	7088Å	
Abell 1446	0.1029	30	13.3(4/30)	24.0(6/25)	7240Å	NS interferes w/OIII
Abell 1684	0.0860	29	3.4(1/29)	33.3(3/9)	7131Å	NS interferes w/H $\beta$ and MgB
Cl1313+073	0.0492	42	9.5(4/42)	0.0(0/17)	6890Å	NS interferes w/H $\beta$
Abell 2214	0.1639	13	0.0(0/13)	0.0(0/8)	7634Å	
Abell 2462	0.0739	48	6.3(3/48)	0.0(0/24)	7050Å	NS interferes w/H $\beta$ and MgB
TOTAL	...	336	8.6(29/336)	9.5(21/221)	...	...

<sup>1</sup>Derived from V $_{\mu}$  in Table 4.

<sup>2</sup>Members include only C1 velocities within  $\approx 4000$  km s $^{-1}$  of the WAT's velocity.

<sup>3</sup>Percentage of member, C1 galaxies with emission lines.

<sup>4</sup>Percentage of non-member, C1 galaxies with emission lines.

<sup>5</sup>Redshifted wavelength of H $\alpha$ .

<sup>6</sup>NS = night sky emission line. The 5577Å and 5195Å NS lines were especially problematic.

<sup>a</sup>Does not include members adopted from literature.

TABLE 7. SPATIAL UNIFORMITY OF MX OBSERVATIONS

Cluster	R <sup>1</sup>	Field <sup>2</sup>	N <sub>exp</sub> <sup>3</sup>	Q1 <sup>4</sup>	Q2	Q3	Q4	In	Out	N <sub>Cand.</sub> <sup>5</sup>	N <sub>Samp</sub> <sup>6</sup>	% <sup>7</sup>	uniform? <sup>8</sup>
Abell 98	3	3.0x5.1	8	57	56	64	73	62	59	253	152	60.0	yes
Abell 160	0	3.7x3.5	13	69	73	54	68	94	54	337	224	66.5	marg,rad
Abell 690	1	3.6x3.6	19	81	79	66	83	74	79	225	172	76.4	yes
Abell 1446	2	3.0x3.0	4	43	42	47	38	34	50	191	81	42.4	yes
Abell 1684	0	2.6x2.6	5	78	67	88	83	58	90	85	66	77.7	marg,rad
Cl1313+073	-0	3.1x3.1	8	62	52	52	62	69	52	190	109	57.4	yes
Cl1919+479	-0	3.0x3.0	13	72	60	88	89	64	86	337	232	76.3	yes
Abell 2214	0	4.3x4.3	4	33	50	78	59	33	67	140	73	52.1	marg,rad
Abell 2220	0	6.3x6.3	3	81	100	58	65	97	65	95	71	74.7	marg
Abell 2462	0	5.2x5.2	8	38	30	31	41	54	19	444	153	34.5	No,rad
Abell 2634	1	3.8x4.3	33	74	74	66	56	90	57	536	368	68.7	No,rad

<sup>1</sup>Abell Richness count.

<sup>2</sup>Search field dimensions in  $h_{75}^{-1}$ Mpc. (The search field was rectangular for A98 because of its bimodal appearance in X-rays.)

<sup>3</sup>Number of 1 hour exposures taken with MX.

<sup>4</sup>Subregion designation: Q1=upper right quadrant, Q2=upper left, Q3=lower left, Q4=lower right, In=inside circle of diameter=1/2 of the field height, Out=outside of this circle.

<sup>5</sup>Number of candidate galaxies in MX catalog.

<sup>6</sup>Number of sampled candidates, i.e., those with at least 1 spectrum.

<sup>7</sup>Percentage of candidates sampled in the entire search field.

<sup>8</sup>Estimate of how evenly the subregions are sampled. No= the sampling percentages are significantly different in some subregions (Poisson statistics), marg= the sampling is only marginally uneven, yes= the sampling is fair and even, rad=the In and Out percentages are significantly different.